



THE UNIVERSITY *of* EDINBURGH

## Edinburgh Research Explorer

### **The relationship between drainage density, erosion rate, and hilltop curvature: implications for sediment transport processes**

**Citation for published version:**

Clubb, F, Mudd, S, Attal, M, Milodowski, D & Grieve, S 2016, 'The relationship between drainage density, erosion rate, and hilltop curvature: implications for sediment transport processes', *Journal of Geophysical Research: Earth Surface*, vol. 121, no. 10. <https://doi.org/10.1002/2015JF003747>

**Digital Object Identifier (DOI):**

[10.1002/2015JF003747](https://doi.org/10.1002/2015JF003747)

**Link:**

[Link to publication record in Edinburgh Research Explorer](#)

**Document Version:**

Peer reviewed version

**Published In:**

Journal of Geophysical Research: Earth Surface

**General rights**

Copyright for the publications made accessible via the Edinburgh Research Explorer is retained by the author(s) and / or other copyright owners and it is a condition of accessing these publications that users recognise and abide by the legal requirements associated with these rights.

**Take down policy**

The University of Edinburgh has made every reasonable effort to ensure that Edinburgh Research Explorer content complies with UK legislation. If you believe that the public display of this file breaches copyright please contact [openaccess@ed.ac.uk](mailto:openaccess@ed.ac.uk) providing details, and we will remove access to the work immediately and investigate your claim.



# The relationship between drainage density, erosion rate, and hilltop curvature: implications for sediment transport processes

Fiona J. Clubb,<sup>1</sup> Simon M. Mudd,<sup>1</sup> Mikael Attal,<sup>1</sup> David T. Milodowski<sup>1</sup>,  
and Stuart W.D. Grieve<sup>1</sup>

---

Corresponding author: Fiona J. Clubb (F.Clubb@ed.ac.uk)

<sup>1</sup>School of Geosciences, University of  
Edinburgh, Drummond Street, Edinburgh,  
United Kingdom, EH8 9XP

This article has been accepted for publication and undergone full peer review but has not been through the copyediting, typesetting, pagination and proofreading process, which may lead to differences between this version and the Version of Record. Please cite this article as doi: 10.1002/2015JF003747

**Abstract.** Drainage density is a fundamental landscape metric describing the extent of the fluvial network. We compare the relationship between drainage density ( $D_d$ ) and erosion rate ( $E$ ) using the Channel-Hillslope Integrated Landscape Development (CHILD) numerical model. We find that varying the channel slope exponent ( $n$ ) in detachment-limited fluvial incision models controls the relationship between  $D_d$  and  $E$ , with  $n > 1$  resulting in increasing  $D_d$  with  $E$  if all other parameters are held constant. This result is consistent when modeling both linear and non-linear hillslope sediment flux. We also test the relationship between  $D_d$  and  $E$  in five soil-mantled landscapes throughout the USA: Feather River, CA; San Gabriel Mountains, CA; Boulder Creek, CO; Guadalupe Mountains, NM; and Bitterroot National Forest, ID. For two of these field sites we compare  $D_d$  to cosmogenic radionuclide (CRN)-derived erosion rates, and for each site we use mean hilltop curvature as a proxy for erosion rate where CRN-derived erosion rates are not available. We find that there is a significant positive relationship between  $D_d$ ,  $E$ , and hilltop curvature across every site, with the exception of the San Gabriel Mountains, CA. This relationship is consistent with an  $n$  exponent greater than 1, suggesting that at higher erosion rates, the transition between advective and diffusive processes occurs at smaller contributing areas in soil-mantled landscapes.

## 1. Introduction

One of the most distinctive features of soil-mantled upland landscapes is the repeating patterns of ridges and valleys. The spacing of these ridges and valleys is fundamentally controlled by the competition between creep-like sediment transport processes, which tend to smooth the landscape, and fluvial processes, which incise the landscape [Tarboton *et al.*, 1992; Tucker and Bras, 1998; Perron *et al.*, 2012]. Perron *et al.* [2008] elegantly demonstrated that the spacing of valleys reflects the relative efficacy of advective (e.g. fluvial) and diffusive (e.g. hillslope) transport processes, both of which may be influenced by climate. Sweeney *et al.* [2015] used laboratory experiments to further demonstrate that the competition between hillslope and valley-forming sediment transport processes controls the degree of landscape dissection. The erosion rate of the landscape plays a major role in controlling the spacing of ridges and valleys, by affecting the relative efficacy of fluvial and hillslope transport processes [Tucker and Bras, 1998; Perron *et al.*, 2008].

How valley spacing, and the associated landscape properties of hillslope length and drainage density ( $D_d$ ), change with erosion rates has been predicted to be sensitive to parameters in common fluvial incision models. Fluvial incision can be modeled using a detachment-limited scenario in which the incision rate  $E$  is a power-law function of upstream drainage area  $A$  and channel slope  $S_{CH}$  [e.g. Whipple and Tucker, 1999]:

$$E = KA^m S_{CH}^n \quad (1)$$

where  $K$  is an erodibility coefficient [ $T^{-1} L^{1-2m}$ ], and  $m$  and  $n$  are constant exponents. The  $m$  and  $n$  exponents in the stream power model have been shown to control the relationship between erosion rate and topographic gradient [Kirkby, 1980, 1993; Howard, 1997; Tucker

and Bras, 1998; Perron *et al.*, 2008]. This relationship has important implications for how landscapes respond to changing tectonic forcing. Royden and Perron [2013] showed analytically that if the parameters are such that the fluvial incision model forecasts a linear relationship between erosion rate and slope, then river profiles will retain features that reflect changes in erosion rates (such as knickpoints). This is assumed in many studies, and means that river profiles can be inverted to obtain uplift histories over millions of years, for example [Roberts and White, 2010; Whittaker *et al.*, 2008], under the assumption that knickpoints are not structurally-controlled. If the relationship is non-linear, however, channels will be imperfect recorders of channel uplift history as the rate of knickpoint migration becomes a function of incision rate [Royden and Perron, 2013]. The value of these parameters in fluvial incision models also controls whether drainage density is sensitive to changing erosion rates [Tucker and Bras, 1998].  $D_d$  also affects the transit time of water through the landscape and thus exerts a primary control on catchment flood response [Chorley and Morgan, 1962; Carlston, 1963; Gregory and Walling, 1968].

Several authors have predicted, based on numerical and analytical models, the relationship between  $D_d$  and metrics describing valley morphology, including slope, erosion rate, and sediment transport process [Kirkby, 1980, 1993; Willgoose *et al.*, 1991; Tucker and Bras, 1998]. Here we build on previous studies that have attempted to examine the relationship between  $D_d$  and erosion rate directly [Montgomery and Dietrich, 1989; Oguchi, 1997; Talling and Sowter, 1999; DiBiase *et al.*, 2012]. These studies used varying methods for identifying the channel to hillslope transition, including slope-area scaling relationships. However, such methods can lack precision due to noise when extracting slope from digital elevation models (DEMs). Recently developed methods of channel head iden-

tification allow the extraction of accurate drainage networks from high-resolution DEMs [Passalacqua *et al.*, 2010a, b, 2012; Pelletier, 2013; Clubb *et al.*, 2014]. In addition, early studies were limited by the coarse resolution of the DEMs available at the time.

In this study we aim to evaluate potential controls on the relationship between drainage density and erosion rate, using both numerical modeling and analysis of real landscapes with high-resolution topographic data. We develop a 1D analytical model using linear and non-linear hillslope sediment flux laws, along with detachment-limited fluvial incision models, to examine the effect of different parameters on the relationship between drainage density and erosion rate. We then use the Channel-Hillslope Integrated Landscape Development (CHILD) model [Tucker *et al.*, 2001] to test our analytical predictions, using both steady-state and transient scenarios. We constrain channel network density using a recently developed technique for extracting channel networks that takes advantage of high-resolution (1 m) light detection and ranging (lidar) datasets in order to test our model predictions on real landscapes. We compare drainage density to basin-averaged erosion rates obtained from detrital cosmogenic radionuclide (CRN) analyses. In sites where CRN-derived erosion rates are not available, we calculate the mean hilltop curvature ( $C_{HT}$ ) of each basin. Mean  $C_{HT}$  has been demonstrated by Hurst *et al.* [2012] to vary linearly with erosion rate in high-relief soil mantled landscapes.

## 2. Theoretical background

The relationship between  $D_d$  and erosion rate can be predicted by combining models of river incision with models of hillslope sediment transport [Tarboton *et al.*, 1992; Tucker and Bras, 1998]. Here we model fluvial incision using the stream power model, a common detachment-limited scenario (equation 1). Depending on the values chosen for the expo-

nents  $m$  and  $n$ , this model can represent fluvial erosion rate as a function of shear stress, for example, or unit stream power [Whipple and Tucker, 1999]. There are significant limitations to this detachment-limited model formulation. It assumes that channel width scales with contributing area, and it does not take into account the effects of sediment flux or the impact of stochasticity and thresholds, all of which can modulate fluvial incision for a given channel geometry [Lague, 2014]. However, Gasparini and Brandon [2011] found that sediment flux and threshold effects can be cast in the general form of equation (1). It is often used to examine fluvial response to changing climatic and tectonic conditions, for example, by solving for the relationship between channel slope and contributing area, assuming uniform incision [Hack, 1973; Flint, 1974; Howard and Kerby, 1983; Sklar and Dietrich, 1998; Wobus et al., 2006]:

$$S_{CH} = \left( \frac{E}{K} \right)^{\frac{1}{n}} A^{-m/n} \quad (2)$$

Choosing correct values of the exponents  $m$  and  $n$  is important in landscape evolution studies, because these values control the relationship between landscape steepness and erosion rates, as well as the competition between advective (fluvial) and diffusive (hillslope) processes. Although the  $m/n$  ratio has been reported for many landscapes [Stock and Montgomery, 1999; Whipple and Tucker, 1999; Anthony and Granger, 2007; Perron and Royden, 2013; Mudd et al., 2014], relatively few studies have reported individual values for the  $m$  and  $n$  exponents, as the erosion rate and  $K$  coefficient must be known. In particular, the slope exponent  $n$  is a critical parameter as it largely controls the timescale and magnitude of fluvial response to perturbations [Whipple and Tucker, 1999]. Howard and Kerby [1983] studied a gradient in erosion rates across badlands in Virginia and suggested values of  $m = 0.45$  and  $n = 0.7$ . Whittaker and Boulton [2012] examined

knickpoint retreat rates above active faults in the Mediterranean and found that increasing channel steepening with fault throw rate may be explained only if the  $n$  exponent is greater than 1.3. *Lague* [2014] reanalyzed data from a range of studies, and suggested that  $m \approx 1$  and  $n \approx 2$  in most cases, with a few exceptions. Data from the Siwaliks in the Himalayas [*Lavé and Avouac*, 2001], Eastern Tibet [*Ouimet et al.*, 2009], and the Mendocino triple junction in the Western USA [*Snyder et al.*, 2000] suggest values of  $m = 0.55$ ,  $0.85$ , and  $2$  and  $n = 1.1$ ,  $1.7$ , and  $4$  respectively [*Lague*, 2014]. *Whipple et al.* [2000] argued that the  $n$  exponent depends on the dominant erosion process and varies between  $\sim 2/3$  and  $\sim 5/3$ . *Royden and Perron* [2013] used transformed river long profiles along with previously-determined uplift rates for the Rio Torto in the central Apennines to estimate an  $n$  value of approximately 0.5. *Mudd et al.* [2014] analyzed the gradient ( $M_\chi$ ) of these transformed profiles to estimate  $0.52 < n < 0.82$  for the Rio Torto. A recent global study of the stream power law parameters by *Harel et al.* [2016] found that in most landscapes the exponent  $n$  is greater than 1.

The  $n$  exponent may be constrained by examining the relationship between  $D_d$  and erosion rate [*Tucker and Bras*, 1998]. We can represent drainage density using the downslope distance from the hilltop to the valley head,  $x_t$ , at which the slopes above and below the valley head are equal. The equilibrium slope for linear hillslope diffusion ( $S_H$ ) can be expressed as [e.g., *Roering et al.*, 2001]:

$$S_H = \frac{E}{D} x_t \quad (3)$$

where  $D$  represents a diffusivity coefficient [ $\text{L}^2 \text{T}^{-1}$ ]. We assume that  $D$  and  $K$  do not vary with erosion rate. In order to equate the channel slope,  $S_{CH}$ , given by equation (2), with  $S_H$ , we assume that the contributing area  $A$  at the channel head is given by a flow



strip of length  $x_t$  [L] and width  $b$  [L], where  $A = x_t b$ :

$$S_{CH} = \left( \frac{E}{Kb^m} \right)^{\frac{1}{n}} x_t^{-m/n} \quad (4)$$

We can equate the slopes above and below the channel head, given by  $S_H$  and  $S_{CH}$  respectively (equations 3 and 4), to obtain the mean length of overland flow:

$$x_t = D^{1/(1+(m/n))} k_f^{-1/(m+n)} E^{(1-n)/(m+n)} \quad (5)$$

where  $k_f = Kb^m$ . This reduces to  $k_f = K [[T^{-1} L^{1-3m}]]$  if we assume a rectangular flow strip of unit width (i.e.,  $b = 1$  m). The mean length of overland flow is approximately equal to half the reciprocal of  $D_d$  [Horton, 1945], and therefore equation (5) can be converted to:

$$\frac{1}{2D_d} = D^{1/(1+(m/n))} K^{-1/(m+n)} E^\alpha \quad (6)$$

where  $\alpha = (1 - n)/(m + n)$ . The relationship between  $D_d$  and erosion rate  $E$  depends on the slope exponent  $n$ , shown in Figure 1a. If  $n > 1$ , the contributing area at the channel head will decrease with increasing erosion rate and  $D_d$  will therefore increase. However if  $n < 1$  then  $D_d$  will decrease with increasing erosion rate [Tucker and Bras, 1998]. Performing a power-law regression on a plot of mean length of overland flow against erosion rate allows the calculation of the  $n$  exponent, assuming the  $m/n$  ratio is known, as  $\alpha$  is the gradient of the regression.

The theory outlined above assumes that hillslope sediment transport occurs by linear diffusion (equation 3). However, in many high-relief landscapes hillslope sediment transport has been suggested to become nonlinear, increasing rapidly as the gradient approaches a critical value [Roering *et al.*, 1999]. Nonlinear hillslope sediment flux ( $Q_c$ ,

$L^3/L/T$ ) can be modeled according to:

$$Q_c = \frac{DS_H}{1 - (S_H/S_c)^2} \quad (7)$$

where  $S_c$  is a threshold slope gradient beyond which  $Q_c$  tends to infinity [Roering *et al.*, 1999, 2001]. Under this regime, hillslope gradient can be stated as [e.g. Roering *et al.*, 2001]:

$$S_H = \frac{DS_c^2}{2Ex_t} \left( \sqrt{1 + \left( \frac{2Ex_t}{DS_c} \right)^2} - 1 \right) \quad (8)$$

Due to the nonlinearity of equation (8), there is no analytical solution equivalent to equation (6). Instead we show numerical results for  $D_d$  as a function of  $E$  in the case of nonlinear hillslope sediment transport in Figure 1b.

Our analytical model outlined above is the simplest case scenario, with a number of assumptions. For example, we assume a linear relationship between  $A$  and  $x_t$ . Alternative model formulations are possible, such as that of a power-law relationship, where  $A = bx_t^y$  [Pelletier *et al.*, 2016]. However, using this alternative power-law relationship predicts the same relationship between  $D_d$  and  $E$  as that of our simpler scenario (see Supporting Information). Furthermore, our model scenario neglects colluvial infilling of the channel head (equation 4). Pelletier *et al.* [2016] present a transport-limited model for predicting drainage density, calibrated for the Walnut Gulch Experimental Watershed, Arizona, where they assume that the channel head occurs where the fluvial erosion rate is greater than the colluvial deposition rate by an amount equal to the net erosion rate  $E$ . In the model outlined above, we follow a similar approach to Tucker and Bras [1998] by assuming that the channel head occurs where the fluvial erosion rate is greater than colluvial erosion. Including colluvial deposition at the channel head in our analytical model

may lead to decreased absolute values of drainage density. In order to test our simple 1D predictions we therefore carried out 2D numerical modeling, described in Section 3.1.

### 3. Methodology

#### 3.1. Landscape evolution modeling

In order to test whether the theory outlined by equations (1) - (8) is applicable in 2D, we analyze a series of model landscape evolution scenarios created using the Channel-Hillslope Integrated Landscape Development (CHILD) model [Tucker *et al.*, 2001]. In the model, topography evolves based on a combination of fluvial incision using the stream power law (equation 1), as well as linear and non-linear diffusive hillslope sediment transport (equations 3 and 7). Our model domain is 500 m by 500 m with a node spacing of 5 m, comparable to the size of the catchments extracted and the DEM resolution of the real datasets respectively. Although the real datasets have a DEM resolution of 1 m, we could not run our numerical models at the same resolution due to computational constraints. Our domain has one boundary set to a fixed elevation ( $z = 0$  m) and three boundaries set to no flux. We detail the model setup and the values of all parameters used in Appendix A and Table 1. We ran three different series of scenarios with different values of  $n$ . Our first scenario set  $n = 1$  and  $m = 0.5$ , where erosion is proportional to specific stream power. We then kept all other parameters constant while changing the value of  $n$ . We ran further scenarios with  $n = 0.4$ ,  $n = 0.7$ , and  $n = 2$ . We chose these values of  $n$  in order to run scenarios with different values of  $\alpha$ . For each scenario, several runs were performed with uplift rates varying between 10 and 320 mm/kyr. We ran each simulation for  $5 \times 10^6$  years to allow the topography to reach steady state, which we determined as occurring when the volume of rock above sea level in the modeled domain became constant. Figures

2a and 2b show examples of the topography generated during these runs with high and low erosion rates. The CHILD model uses a triangulated irregular network (TIN). We converted the output TINs to rasters and performed the same topographic analysis as with the real datasets, described in the following sections. We extracted the channel network and calculated the drainage density for the whole catchment generated; the methodology for channel extraction is described in Section 3.4. We also computed mean  $C_{HT}$  for each run following the methodology outlined in Section 3.5. We further wished to examine the effect of different hillslope transport laws on the relationship between  $D_d$  and  $C_{HT}$  for varying values of  $n$ . Therefore all our steady-state scenarios have been run twice, using linear and non-linear hillslope sediment flux laws (equations (3) and (7), respectively).

In addition to steady state runs, we examined a transient scenario for three values of  $n$ :  $n = 1$ ,  $n = 2$ , and  $n = 0.7$  with linear hillslope sediment transport. We ran these scenarios to test whether such landscapes conform to the same theory, and whether spatial changes in drainage density resulting from varying erosion rates can be detected. These were performed with a larger model domain (2000 m by 2000 m) in order to examine the variation in drainage density across different basins in the same landscape (Figure 2c).

The model was run at a low uplift rate (40 mm/kyr) for  $20 \times 10^6$  years, then the uplift rate was increased to 320 mm/kyr for  $1 \times 10^6$  years. This allowed us to compare basins responding to different uplift rates in the same model landscape. Our transient scenarios were analyzed following the same procedures (Sections 3.4 and 3.5), with the drainage density and hilltop curvature extracted for different basins in the domain.

A potential limitation of using the CHILD model is that the hillslope sediment transport term does not account for flow width (equation 3) [Howard, 1994; Pelletier, 2010].

*Pelletier* [2010] suggested that, if the grid resolution of the model ( $\delta$ ) is greater than that of the valley width ( $w$ ), the diffusive transport term should be scaled by a ratio of  $\delta/w$ . This is not accounted for in CHILD, suggesting that our model runs may underestimate the colluvial deposition rate and potentially predict higher drainage densities. In order to test the sensitivity of our model scenarios to grid resolution, we ran our steady-state scenarios at grid resolutions of 2.5 m, 7.5 m, and 10 m, along with the original 5 m runs. We found that the predicted relationship between  $D_d$  and  $E$  was independent of grid resolution (Supporting Figures S3 to S5).

### 3.2. Study areas

As well as testing our predictions on model landscapes, we report  $D_d$  and hilltop curvature for five field sites with 1 m resolution lidar data: two sites in California, one site in Colorado, one site in New Mexico, and one site in Idaho (Figure 3). These sites were chosen based on the following criteria: (i) the availability of 1 m resolution lidar data; (ii) relatively uniform lithology across the site; and (iii) a gradient in erosion rates across the landscape, either measured or inferred based on highly variable slopes and ridgetop curvatures. Table 2 summarizes the mean annual temperature and mean annual precipitation of each site [PRISM Climate Group, <http://prism.oregonstate.edu>], the underlying lithology, and the elevation range. These sites are predominantly soil-mantled, as shown in Table 2, although some of these sites have bedrock outcrops, such as the Guadalupe Mountains and the San Gabriel Mountains, which becomes bedrock-dominated in the rapidly eroding parts of the landscape [*DiBiase et al.*, 2010]. Debris flows are also prevalent at the San Gabriel Mountains site [*DiBiase et al.*, 2012].

### 3.3. Cosmogenic radionuclide (CRN)-derived erosion rates and study basins

In order to examine the relationship between  $D_d$  and erosion rate, published CRN-derived erosion rates were compiled from two sites: Feather River, CA [Riebe *et al.*, 2000; Hurst *et al.*, 2012] and Boulder Creek, CO [Dethier *et al.*, 2014] summarized in Table 3. No CRN data are available for the other sites. The catchment-averaged erosion rates for the Feather River field site were derived using  $^{10}\text{Be}$  concentrations from fluvial sands, assumed to have minimal storage in the fluvial system, by Riebe *et al.* [2000] and Hurst *et al.* [2012]. A total of 21 CRN-derived erosion rates are available for the Feather River. These erosion rates span an order of magnitude, varying from  $12.5 \pm 1.4$  mm/kyr to  $253.8 \pm 66.6$  mm/kyr. CRN-derived erosion rates for the Boulder Creek field site were also calculated by measuring  $^{10}\text{Be}$  concentrations from quartz in alluvial channel sediments by Dethier *et al.* [2014]. Within the Boulder Creek catchment there are twelve basins for which a CRN-derived erosion rate is available, ranging from  $14.97 \pm 1.25$  mm/kyr to  $62.92 \pm 5.96$  mm/kyr.

Two sets of study basins were used in the analysis. The first set of study basins included all catchments for which there were CRN-derived erosion rates available (the two sites above). The second set of study basins, extracted for each of the five sites, included all third order basins. We chose to use third order basins to sample across a large number of catchments at different erosion rates in each site. We obtained the mean hilltop curvature for each of these basins to use as a proxy for erosion rate where CRN-derived erosion rates were not available, as previous work by Hurst *et al.* [2012] demonstrated that hilltop curvature scales linearly with erosion rate.

### 3.4. Drainage density

$D_d$  was calculated for each of the study basins using the DrEICH method, a channel head extraction algorithm [Clubb *et al.*, 2014]. The DrEICH method extracts channel heads based on transforming river profiles into  $\chi$ -elevation space [Perron and Royden, 2013], identifying the upstream transition between fluvial and hillslope processes [Clubb *et al.*, 2014]. Perron and Royden [2013] showed that river profiles are linearized when transformed into  $\chi$ -elevation space. The DrEICH algorithm identifies channel heads as the point at which these profiles become non-linear, representing the transition to hillslope processes [Clubb *et al.*, 2014]. In order to extract channel networks for each field site via the DrEICH methodology, the  $m/n$  value for the landscape must be calculated. This was done using the independent statistical collinearity tests described by Mudd *et al.* [2014] which assume channel profiles are made up of a number of different segments depending on heterogeneities and spatial variations in incision rate within the river profile. The collinearity test loops through all potential  $m/n$  values and performs a piecewise linear regression on the profile. For each regression the Akaike information criterion (AIC) is calculated [Akaike, 1974], which measures how well the data fit the regression whilst penalizing for over-fitting. The best fit  $m/n$  is selected at the minimum AIC value.

We ran the test described by Mudd *et al.* [2014] on two catchments at each field site using 10 m DEMs derived from the United States Geological Survey's National Elevation Dataset. We used the National Elevation Dataset instead of the lidar data at each field site to provide a larger area for calculation of the  $m/n$  ratio and to reduce computational cost. The Mudd *et al.* [2014] algorithms require four user-defined parameters: the target skip value, the standard deviation of the elevation data ( $\sigma$ ), the minimum segment length, and the number of target nodes (for a detailed description of each of these parameters see

*Mudd et al.* [2014]). The value of these parameters can influence the result of the  $m/n$  analysis. We performed a sensitivity analysis by changing each parameter and examining the variation in  $m/n$  ratios extracted. In total we ran 54 combinations of the parameters to determine the best fit  $m/n$ . We varied the skip parameter between 1 and 3, the number of target nodes between 80 and 100, and the minimum segment length between 10 and 20 nodes. We used a  $\sigma$  value of 3 m for all field sites, as analyses performed by *Mudd et al.* [2014] showed that the most reliable  $m/n$  ratios were calculated when  $\sigma$  values were  $\leq 3$  m. We used the mean value of the sensitivity analyses as the best fit  $m/n$  for the sites; mean, median and standard deviation of the analyses are reported in Table 4.

The DrEICH algorithm first identifies concave portions of the landscape using a curvature threshold, which is calculated using the quantile-quantile method of *Passalacqua et al.* [2010a]. First of all, the DEM is smoothed using optimal Wiener filtering, which distinguishes the large scale signal of the fluvial-hillslope system from microtopographic noise [*Pelletier*, 2013]. After smoothing the DEM, the curvature threshold is calculated based on a quantile-quantile plot of the distribution of curvature in each landscape (for more details on this methodology see *Passalacqua et al.* [2010a, b, 2012]). The DrEICH algorithm identifies the upstream extent of fluvial incision within the valleys based on  $\chi$ -transformed longitudinal profiles [*Clubb et al.*, 2014]. It assumes that the channel profile will be made up of two segments in  $\chi$ -elevation space: a linear channel segment and a non-linear hillslope segment. The channel head in each valley is calculated as the transition point between the best-fit linear channel segment and non-linear hillslope segment. The DrEICH algorithm was tested against 167 field-mapped channel heads from a variety of landscapes by *Clubb et al.* [2014], and was found to accurately reproduce the field-mapped



channel networks when compared to other channel extraction methods. Our analytical model described in Section 2 relies on equating the channel and hillslope gradient at the channel head. In order to test whether these were comparable, we extracted the gradient 2 m above and below each channel head for every field site, and calculated the percentage difference between the two gradients. We then calculated the mean percentage difference across each landscape (Table 2). For each field site there was less than 25% mean difference in the gradients above and below the channel heads, suggesting that our assumption of equating the slopes in our analytical model is valid.

For each basin of interest, we then extracted the total length of channels via the DrE-ICH method, and divided it by the basin contributing area to calculate the  $D_d$  (expressed in  $\text{m}/\text{m}^2$ ). We extracted the drainage density for two different sets of basins: all basins with CRN-derived erosion rates where these were available (the Feather River and Boulder Creek field sites), and all third order basins for every field site to investigate the relationship between  $D_d$  and mean  $C_{HT}$ .

### 3.5. Mean hilltop curvature

Mean  $C_{HT}$  may be used to infer the distribution of erosion rates across the landscape [Roering *et al.*, 2007; Hurst *et al.*, 2012]. Hurst *et al.* [2012] demonstrated that mean  $C_{HT}$  continues to vary linearly with erosion rate after hillslope gradient has become insensitive to increasing erosion rate. Mean  $C_{HT}$  has been demonstrated to respond rapidly to changing channel steepness in soil-mantled landscapes, and can therefore be used as a proxy for erosion rate in areas where CRN-derived erosion rates are not available [Hurst *et al.*, 2013a]. In order to ensure our landscapes were dominantly soil-mantled, we calculated the percentage of ridgetops that were soil-mantled in each field site using the surface rough-

ness algorithm described in *Milodowski et al.* [2015a]. We detect patches of bedrock from our lidar DEMs, using a surface roughness ratio of 0.015 as the threshold for bedrock, following *Milodowski et al.* [2015a]. The roughness ratio is a measure of the local variability of the surface normal vectors, which has been shown to correspond to the outcrop of bedrock [*Milodowski et al.*, 2015a]. The percentage of ridgetops identified as soil-mantled are reported in Table 2, and is  $\geq 70\%$  for every field site. In some circumstances,  $C_{HT}$  may not reflect the variability of erosion rates across the landscape. In transient landscapes, some basins may contain knickpoints, leading to differing erosion rates within the same basin. Therefore, hilltops connected to the channel above and below the knickpoint may not be adjusted to the same channel incision rate [e.g., *Mudd and Furbish*, 2007; *Reinhardt et al.*, 2007; *Anderson et al.*, 2012; *Hurst et al.*, 2012, 2013a]. In addition, the presence of landslides in some high-relief basins may lead to decoupling of hilltops from the channel network. To avoid such issues, we visually excluded basins with landslides or knickpoints evident from the lidar DEM.

Ridgetops were mapped as the intersecting margins of basins from zeroth stream order and upwards, following the methodology of *Hurst et al.* [2012] and *Grieve et al.* [2016a]. Only hilltops internal to each study basin were considered, in order to ensure that  $C_{HT}$  was adjusted to the erosion rate within each basin. Curvature was calculated using polynomial surface fitting with a circular window radius of 7 m [*Hurst et al.*, 2012]. The polynomial surface has the form:

$$z = ax^2 + by^2 + cxy + dx + ey + f \quad (9)$$

where curvature ( $C$ ) and slope ( $S$ ) can be determined from the fitted coefficients:

$$C = 2a + 2b \quad (10a)$$

$$S = \sqrt{d^2 + e^2} \quad (10b)$$

The size of the window radius is determined through identifying scaling breaks in the interquartile range and standard deviation of the curvature [Lashermes *et al.*, 2007; Roering *et al.*, 2010; Hurst *et al.*, 2012]. This ensures that curvature is sampled over a length scale characteristic of hillslope to valley transitions. Mean  $C_{HT}$  was computed for each third order basin. The relationship between  $C_{HT}$  and  $D_d$  was then examined across each field site.

### 3.6. Constraints on the $n$ exponent

Theoretically the  $n$  exponent in the detachment-limited incision model (equation 1) may be calculated using the relationship between the mean length of overland flow (inversely proportional to drainage density) and the erosion rate, if known. We fitted a power-law to the relationship between mean length of overland flow and erosion rate for the two field sites with CRN-derived erosion rates available: Feather River, California, and Boulder Creek, Colorado. We used the gradient of the regression,  $\alpha$  to calculate the  $n$  exponent based on equation (6).

## 4. Results

### 4.1. Landscape evolution modeling

For each of the steady state modeling scenarios ( $n = 0.4$ ,  $n = 0.7$ ,  $n = 1$ , and  $n = 2$ ) the relationship between  $D_d$  and uplift rate was plotted for both linear and non-linear hillslope sediment transport (Figures 4 and 5). Figure 4 shows that in the scenarios

with linear hillslope sediment transport, there is a positive relationship between drainage density and uplift rate (and therefore erosion rate as the scenarios are at steady state) for  $n = 2$ ; a negative relationship for  $n = 0.7$  and  $n = 0.4$ ; and that drainage density is invariant with uplift rate for  $n = 1$ . The negative relationship between  $D_d$  and  $U$  is steeper for  $n = 0.4$  than  $n = 0.7$ , as would be expected from equation (6) and Figure 1. We fit a linear regression to the relationship between hilltop curvature and uplift rate based on the predictions of erosion rate and mean  $C_{HT}$  set out by *Roering et al.* [2007] and following the methodology of *Hurst et al.* [2012], shown in Figure 6. We find a significant positive relationship between mean  $C_{HT}$  and uplift rate for both the linear and non-linear hillslope sediment transport scenarios. These results in an ideal landscape mirror those from our theory (Section 2) and justify the use of  $C_{HT}$  as an indicator of erosion rate in soil-mantled landscapes. The same general trends between  $D_d$  and  $U$  are apparent for non-linear sediment transport (Figure 5). Figure 1b suggests that the relationship between  $D_d$  and uplift rate should be steeper for  $n = 2$  for non-linear sediment transport, which is not evident from our modeling results. Our transient simulations (Figure 7) show the same trends as our steady-state runs, suggesting that the same theory can be applied to transient landscapes.

#### 4.2. CRN-derived erosion rates and drainage density

For our real landscapes, we created scatter plots of  $D_d$  against CRN-derived erosion rates for the two field sites with available CRN data: Feather River, CA, and Boulder Creek, CO. A power-law regression was fitted to the raw data for each of the field sites (Figure 8). A regression was deemed to be significant if the  $p$  value was less than 0.01 (99% confidence interval). Figure 8 shows that for both the Feather River and Boulder Creek

field sites there is a positive relationship between erosion rate and  $D_d$ . The regressions for the Feather River and Boulder Creek both have  $p$  values  $<0.01$ , and  $R^2$  values of 0.76 and 0.82 respectively. The exponents on the power-law relationships ( $\alpha$ ) are 0.91 and 1.37 respectively.

#### 4.3. Mean hilltop curvature and drainage density

Mean hilltop curvature was calculated for every third order basin in each of the five study sites and compared to drainage density. Figure 9 shows an example of the spatial distribution of hilltop curvature and drainage density for the Guadalupe Mountains field site. Scatter plots were created of  $D_d$  against mean  $C_{HT}$  for each of these basins (Figure 10), and the data were also binned with a bin width of  $0.005 \text{ m}^{-1}$ . A power-law relationship was fit through all of the data points for each field site, and the  $p$  value and  $R^2$  were reported (see Figure 10). A significant positive relationship between mean  $C_{HT}$  and  $D_d$  was observed for four out of the five field sites analyzed in this study, with the exponent in the power-law relationship varying between 0.15 and 0.6. There was no significant relationship observed between  $C_{HT}$  and  $D_d$  for the San Gabriel Mountains field site, with a  $p$  value of 0.02 and an  $R^2$  of 0.18. Mean  $C_{HT}$  may only be used as a proxy for erosion rate if the ridgetops are soil-mantled. Therefore the percentage of bedrock ridgetops as a function of mean  $C_{HT}$  was also plotted for each field site (Figure 11). We found a positive linear relationship between the percentage of bedrock ridgetops and mean  $C_{HT}$  for each field site. The vast majority of basins in each site had a low percentage of bedrock ridgetops (Figure 11), although one basin in the Bitterroot National Forest site had an anomalously high percentage (70%).

#### 4.4. Constraints on the $n$ exponent

The relationship between  $D_d$  and erosion rate can theoretically be used to calculate the  $n$  exponent. The scatter plots of  $D_d$  against CRN-derived erosion rate show a positive relationship for the Feather River and Boulder Creek (Figure 8). Furthermore, there is also a positive relationship between  $D_d$  and mean  $C_{HT}$  for four out of the five field sites (Figure 10). This suggests that  $n > 1$  at each of these sites. We can use the relationship between the mean length of overland flow (inversely proportional to  $D_d$ ) and erosion rate to calculate  $n$  if the  $m/n$  ratio is known using equation (6). However, we find that varying the gradient of the regression within the range of acceptable values results in a wide variation in the calculated  $n$  exponent. Therefore it was not possible to further constrain the value of the  $n$  exponent using this technique.

#### 5. Discussion

The results of our landscape evolution modeling show that the theoretical concepts outlined in Section 2 are applicable in a 2D domain. We find that the nature of the relationship between  $D_d$  and  $E$  in our model scenarios vary with the value of the slope exponent in the detachment-limited incision model,  $n$ . Our steady state modeling runs (Figures 4 - 5) show that if  $n > 1$ , there is a positive relationship between  $D_d$  and  $C_{HT}$ , whereas if  $n < 1$  there is a negative relationship. Our modeling of transient scenarios also supports this, showing that the theory is still applicable in these landscapes. There was a significant trend between drainage density and mean hilltop curvature for our transient model runs with  $n = 0.7$  and  $n = 2$ , with  $R^2$  values of 0.85 and 0.58 respectively (Figure 7).

Our modeling results also have implications for examining the impact of non-linear hillslope sediment transport on length scales in landscapes. As relief increases and hillslopes approach threshold gradients, hillslope sediment transport becomes increasingly non-linear, as sediment flux becomes dominated by mass wasting and landslides [Roering *et al.*, 1999]. Our landscape evolution modeling scenarios where hillslope sediment transport was non-linear (Figure 5) exhibited the same relationships between drainage density and erosion rate as scenarios in which hillslope sediment transport was linear. However, our analytical solution (Figure 1) predicted a steeper relationship between  $D_d$  and uplift rate with non-linear transport for  $n = 2$ . This may be due to noise in our modeling results (Figures 4 - 7). This noise may be caused by the extraction of hilltop curvature from the model domain, as well as the loss of information when transforming a TIN network onto a regular grid. The model has a grid spacing of 5 m due to computational constraints, but this resolution may not be fine enough to perfectly capture the variation in curvature along the ridgetops. Despite the noise, a clear significant trend between drainage density and uplift rate is observed from the steady state model runs using linear and non-linear sediment flux laws, with  $R^2$  values ranging from 0.88 - 0.96. (Figures 4 - 5).

It may be expected that the effect of the non-linear sediment flux law will increase with erosion rates in higher-relief landscapes. In our CHILD model runs we tested a maximum erosion rate of 320 mm/kyr in order to compare these results to our real landscapes with CRN-derived erosion rates in this order of magnitude (Table 3). At higher erosion rates, where landscapes transition from soil-mantled to bedrock-dominated,  $C_{HT}$  cannot be used as an indicator of erosion rate as soil production can no longer keep pace with transport rates [Hurst *et al.*, 2012]. Therefore the results of our study are applicable to

landscapes with soil-mantled ridgetops where  $C_{HT}$  can be used as a proxy for erosion rate across the landscape. Figure 11 shows that in each field site with the exception of Bitterroot National Forest, the majority of basins had below 20% of ridges identified as bedrock. In the Bitterroot site the majority of basins had less than 35% bedrock ridgetops, although with more variability than the other field sites. This may lead to more noise in the relationship between  $D_d$  and  $C_{HT}$  in this site, although a significant positive relationship was still observed (Figure 10). In regions with much higher erosion rates, a positive relationship between  $D_d$  and erosion rate may not be observed. Previous studies by *Oguchi* [1997] in the mountainous region of central Japan, and by *Talling and Sowter* [1999] in the Southern San Joaquin Valley, California, found lower drainage densities corresponding to higher relief. These authors concluded that the dominance of mass-wasting processes on steep slopes in these regions resulted in a negative relationship between  $D_d$  and relief. In contrast, *Sangireddy et al.* [2016] found that across a wide range of humid landscapes  $D_d$  was positively correlated with relief.

We also tested our predictions on real landscapes, using lidar-derived DEMs for five field sites in the USA. Our results show a positive relationship between  $D_d$  and erosion rate, using CRN-derived erosion rates for two of the field sites, and mean  $C_{HT}$  for four out of the five sites. Drainage density has profound implications for the transit time of runoff through catchments, and maximum storm runoff has been demonstrated to be a function of drainage density [*Chorley and Morgan*, 1962; *Gregory and Walling*, 1968]. Our results suggest that increasing erosion rates will therefore result in more rapid catchment response to storms or precipitation events. Furthermore, an increase in drainage density with erosion rate may increase the rapidity of sediment supply to the fluvial network.



This is an important control on downstream fluvial morphology, influencing the transition between braided and meandering channels, for example, as stable meandering channels are more likely to develop with low rates of sediment transport [Church, 2006]. Furthermore, based on our landscape evolution modeling results, this positive relationship between drainage density and erosion rate is consistent with a value of  $n$  in the stream power law (equation 1) greater than 1. In landscapes with linear hillslope sediment transport, if  $n$  is greater than 1 and other parameters are constant, as slope increases (in response to an increase in uplift, for example) fluvial processes will out-compete diffusive processes. This would lead to channel incision occurring further upstream and an increase in  $D_d$ . However, where hillslope sediment transport is non-linear, this relative efficiency of advective and diffusive processes may also depend on the critical gradient,  $S_c$ . We set  $S_c$  constant in our modeling scenarios but acknowledge that the value of  $S_c$  may vary spatially [Grieve *et al.*, 2016a, b], which could affect the observed relationship between drainage density and erosion rate.

The value of the  $n$  exponent also has important implications for how the landscape responds to transient forcing. The slope of river profiles may be used to extract information about the uplift history of the channel [Pritchard *et al.*, 2009; Roberts and White, 2010]. However, complete uplift histories can only be extracted from channel profiles if  $n = 1$ , when knickpoint retreat rates should be independent of erosion rate. Royden and Perron [2013] demonstrated that if  $n > 1$ , rapid incision signals should propagate upstream more rapidly than slow incision (with the converse true for  $n < 1$ ). Steep segments in river profiles are predicted to lengthen when  $n > 1$ , consuming lower gradient segments and therefore progressively destroying the record of the preceding uplift history. Our results

are consistent with  $n > 1$  for four of the field sites analyzed, and  $n \geq 1$  for all of the field sites. This agrees with *Laque* [2014], who found that  $n \approx 2$  in the majority of cases. Our results therefore imply that channels in these landscapes will be imperfect recorders of tectonic forcing, and complete uplift histories cannot be extracted from these river profiles.

The competition between the parameters  $D$  and  $K$  has been shown to exert a first order control on valley spacing [e.g. *Perron et al.*, 2008, 2009; *Sweeney et al.*, 2015]. *Perron et al.* [2008] showed that valley spacing is also predicted to vary with the parameters  $m$ ,  $n$ , and relief ( $\zeta$ ). They define the Peclet number,  $Pe$  as:

$$Pe = \frac{Kl^{2(m+1)-n}}{D\zeta^{1-n}} \quad (11)$$

where  $l$  is the horizontal length of a drainage basin. *Perron et al.* [2008] suggest that, assuming the other parameters are constant, higher erosion rates will increase  $Pe$  through an increase in relief,  $\zeta$ , if  $n > 1$ . This leads to narrower valley spacing and increased drainage density. However, if  $n = 1$ ,  $Pe$  is independent of relief. This theory is consistent of the results of our study, where we find that a positive relationship between drainage density and erosion rate, consistent with  $n > 1$ .

However, a key assumption of our study is that the  $D$  and  $K$  parameters in equations (1) and (3) are constant. The competition between these parameters has been shown to exert a first order control on valley spacing [e.g. *Perron et al.*, 2008, 2009; *Sweeney et al.*, 2015]. However, the values of  $D$  and  $K$  may vary both spatially and temporally. The hillslope diffusion coefficient,  $D$ , is a function of hillslope sediment properties, such as soil thickness, cohesion, and grain size [*Furbish et al.*, 2009]. Both soil thickness and grain size are thought to vary with erosion rate [*Heimsath et al.*, 1997; *Attal et al.*, 2015;

*Riebe et al.*, 2015].  $D$  has also been shown to vary with climate through controls on soil transport processes [e.g. *Carson and Kirkby*, 1972; *Yoo et al.*, 2005], and lithology, which affects material properties and soil particle sizes [*Hurst et al.*, 2013b]. If soil thickness decreases with erosion rate, the models of depth-dependent sediment transport suggest that  $D$  may also vary with erosion rate [e.g. *Braun et al.*, 2001]. The channel erodibility coefficient,  $K$ , is a function of many parameters such as lithology, climate, sediment cover, and channel width [*Whipple and Tucker*, 1999].  $K$  may vary with erosion rate through channel width adjustments, as channels have been demonstrated to narrow in response to steepened reaches from increased uplift rates [e.g. *Finnegan et al.*, 2005; *Amos and Burbank*, 2007]. If  $n = 1$  then equation (6) simplifies so that  $D_d$  is dependent on  $D/K$ . This suggests that, if  $n = 1$ , a positive relationship between  $D_d$  and  $E$  may result from a decreasing  $D/K$  ratio with erosion rate (Figure S2, Supporting Information). This may be caused by a decrease in  $D$ ; an increase in  $K$ ; or  $K$  increasing faster than  $D$  such that the ratio decreases. However, as no field evidence has demonstrated how  $K$  or  $D$  vary with  $E$ , these three scenarios cannot be distinguished. With these limitations, we suggest that our results are consistent with the hypothesis that  $n > 1$  for four out of the five field sites, although acknowledge that there may be other possible explanations for the observed relationship.

A further assumption of our analytical predictions is that of detachment-limited fluvial incision (see equation 1). Detachment-limited incision assumes that the erosion rate is related to the shear stress, velocity, or power of overland flow, and that sediment is transported by the channel without being deposited. It has been assumed in many studies modeling evolution of soil-mantled landscapes [e.g. *Howard*, 1994, 1997; *Perron et al.*,

2008, 2009]. Other studies, however, suggest that erosion in soil-mantled landscapes is transport-limited, where erosion rate is proportional to the divergence of sediment flux [e.g. *Tucker and Bras*, 1998; *Simpson and Schlunegger*, 2003; *Istanbulluoglu et al.*, 2003]. *Pelletier* [2012] demonstrated through analysis of field measurements, along with numerical modeling, that at small spatial scales, both detachment- and transport-limited conditions may apply depending on the texture of the eroding soil. The assumption of detachment-limited conditions is a simplifying one that we make in this study to generate simple predictions that are testable against our real landscapes. However, *Tucker and Bras* [1998] present a purely transport-limited model of the drainage density in soil-mantled landscapes, and predict similar relationships between  $D_d$  and  $E$  as we find in our detachment-limited model.

Previous studies have suggested that the underlying lithology has an effect on  $D_d$  [*Oguchi*, 1997]. Three of the sites analyzed (Feather River, Boulder Creek, and the San Gabriel Mountains) were situated on granitic lithologies; the Guadalupe Mountains site was primarily composed of limestone; and the Bitterroot National Forest site was composed of schist and gneissic bedrock. Despite these variations, the relationship between  $D_d$  and erosion rate was positive for four of these sites (Figures 8 and 10). The San Gabriel Mountains is the only site to show no relationship between drainage density and erosion rate. *DiBiase et al.* [2012] analyzed the same DEM, and found that fluvial drainage density decreased with increasing erosion rate, while colluvial channels become denser, leading to the total drainage density remaining constant across the landscape. This contrasts with our analysis, as we found that fluvial drainage density was invariant with erosion rate. The difference between these results may be due differences in channel extraction: *DiBi-*

*ase et al.* [2012] used slope-area plots to identify fluvial channels, whereas in our analysis we used the DrEICH algorithm, which identifies channels based on transformed river long profiles. Our results are consistent with the  $n$  value in this landscape being close to 1, as implied by our numerical modeling results. As shown by the San Gabriel Mountains site, the presence of colluvial channels in steep landscapes formed through debris flow processes [Stock and Dietrich, 2003] may complicate the results of our analysis. These colluvial channels can impact the results of channel extraction algorithms, and therefore the calculation of drainage density across the landscape, as the DrEICH algorithm is focused on identifying the extent of the fluvial channel network.

Furthermore, although we link changing drainage density to erosion rate, there are various other factors in the landscape that may affect both  $D_d$  and  $E$ . Several landscape metrics have been shown to vary with erosion rate, such as soil thickness [Heimsath et al., 1997, 2012; Gabet et al., 2015] and vegetation [Milodowski et al., 2015b]. In many landscapes, sediment flux has been suggested to be depth-dependent [Heimsath et al., 2005; Roering, 2008], and bioturbation efficiency may be reduced as the amount of biomass supported by the landscape decreases [Gabet et al., 2003]. Reduced vegetation cover may also result in increased susceptibility to erosion by overland flow [Istanbulluoglu and Bras, 2005]. Therefore, while we attribute changes in drainage density to fluvial processes, we acknowledge that drainage density variations may be driven by other processes. Although these factors may complicate the interpretation, we observe a consistent trend between drainage density and erosion rate across four of our sites, which vary from low-relief landscapes, such as Guadalupe Mountains, to higher-relief landscapes, such as the Bitterroot National Forest and Boulder Creek sites.

## 6. Conclusions

Our results show a consistent positive relationship between  $D_d$  and erosion rate across four field sites in the USA with varying lithologies and climates. We compared  $D_d$  with CRN-derived erosion rates at two field sites; and with hilltop curvature at all field sites. There was a significant positive relationship between  $D_d$  and CRN-derived erosion rates, as well as with  $C_{HT}$ , whereas one field site demonstrated no relationship between  $D_d$  and mean  $C_{HT}$ . Our modeling results confirm that  $C_{HT}$  may be used to reflect the spatial variability of erosion rates across multiple landscapes [Hurst *et al.*, 2012]. The positive relationship between  $D_d$  and erosion rate constrains fundamental parameters in theoretical models of fluvial incision, particularly the  $n$  exponent. Our results are consistent with a value of  $n$  exceeding unity across four of our sites, assuming that  $K$  and  $D$  are invariant with erosion rate. This suggests that, all else being equal, advection out-competes diffusion in higher-relief landscapes, leading to fluvial incision occurring further up-valleys and resulting in an increase in  $D_d$ . However, this relationship may not be apparent in landscapes dominated by debris flow processes, such as in the San Gabriel Mountains site. Furthermore, river profiles will not be perfect recorders of uplift histories in landscapes where  $n > 1$ , as more rapidly eroding reaches will migrate upstream at a faster rate, progressively consuming the erosion history encoded into the upstream portion of the channel network [Royden and Perron, 2013]. We constrain our topographic analysis with landscape evolution modeling, which shows that both linear and non-linear hillslope sediment transport predict similar relationships between drainage density and erosion rate at steady state within the range of erosion rates tested. We also test a

transient scenario of rapid uplift with linear hillslope sediment transport, showing the same predicted relationships to that of the steady state scenarios.

## Appendix A: Description of parameters used in the CHILD model

In the CHILD model, topography evolves based on equation (1), and either equation (3) or equation (7) [Tucker *et al.*, 2001; Attal *et al.*, 2011]. The scenarios we present model purely detachment-limited erosion, where there are neither erosion thresholds nor adjustment in channel geometry. Erosion driven by soil creep is computed based on equation (3). We also examine scenarios where hillslope erosion is driven by nonlinear sediment flux, calculated by equation (7). Fluvial erosion rate  $E$  [L T<sup>-1</sup>] is calculated following:

$$E = k_b \tau^{pb} \quad (\text{A1})$$

where  $k_b$  is a specific bedrock erodibility coefficient (in L T<sup>-1</sup> per “stress quantity” in SI units),  $\tau$  [M L<sup>-1</sup> T<sup>-2</sup>] is a fluvial shear stress quantity, and  $pb$  is a dimensionless constant. The erosion rate calculated for both hillslope and fluvial processes is compared at each time step for each node, and the elevation of the node is lowered by the largest amount predicted by either of the two processes. Beyond a given contributing area, fluvial processes become dominant, and equation (A1) prevails. The shear stress quantity (the unit of which depends on the values chosen for exponents  $mb$  and  $nb$ ) is calculated according to:

$$\tau = k_t (Q/W)^{mb} S^{nb} \quad (\text{A2})$$

where  $Q$  is water discharge [L<sup>3</sup> T<sup>-1</sup>],  $W$  [L] is channel width,  $k_t$  is a coefficient, and  $mb$  and  $nb$  are constants. Here, channel width is calculated using the simplest form of hydraulic

scaling available in CHILD [*Leopold and Maddock, 1953*]:

$$W = k_w Q^{1/2} \quad (\text{A3})$$

where  $k_w$  is a hydraulic scaling coefficient [ $\text{L}^{-1/2} \text{T}^{1/2}$ ]. In the model, we assume no infiltration so that discharge is only the product of precipitation rate  $P$  in [ $\text{L T}^{-1}$ ] by contributing area:

$$Q = PA \quad (\text{A4})$$

Combining equations (A1) to (A4) gives:

$$E = k_b k_t^{pb} k_w^{(pb.mb)} P^{(pb.mb/2)} A^{(pb.mb/2)} S^{(pb.nb)} \quad (\text{A5})$$

This equation is equivalent to equation (1), with  $m = pb.mb/2$ ,  $n = pb.nb$ , and  $K = k_b k_t^{pb} k_w^{(-pb.mb)} P^{(pb.mb/2)}$ . Note that the exponents  $mb$ ,  $nb$ , and  $pb$  can be set to simulate different fluvial incision laws (i.e. incision rate proportional to fluvial shear stress, cross-section-averaged stream power, or specific stream power). We start our initial scenario with  $nb = mb = pb = 1$  where erosion is proportional to specific stream power. This leads to  $m = 0.5$  and  $n = 1$  in equation (1). We then vary  $n$  in each scenario, while leaving  $m$  constant. Table 1 details the value of each parameter in the model runs.

**Acknowledgments.** FJC is supported by the Carnegie Trust for the Universities of Scotland. SMM and SWDG are supported by NERC grant NE/J009970/1 and SMM is supported by U.S. Army Research Office contract number W911NF-13-1-0478. DTM is supported by NERC grant NE/J500021/1. The authors would like to thank Greg Tucker for advice on CHILD simulations, along with Jon Pelletier and two anonymous reviewers for their comments and suggestions. All DEMs used in the study are freely available online from [www.opentopography.org](http://www.opentopography.org), and the code used to extract the channel networks



and calculate the drainage density (the DrEICH algorithm) is available to download via GitHub at <https://github.com/LSDtopotools/>.

## References

- Akaike, H. (1974), A new look at the statistical model identification, *Automatic Control, IEEE Transactions on*, 19(6), 716–723, doi:10.1109/tac.1974.1100705.
- Amos, C. B., and D. W. Burbank (2007), Channel width response to differential uplift, *Journal of Geophysical Research: Earth Surface*, 112(F2), F02,010, doi:10.1029/2006JF000672.
- Anderson, S. P., R. S. Anderson, and G. E. Tucker (2012), Landscape scale linkages in critical zone evolution, *Comptes Rendus Geoscience*, 344(1112), 586–596, doi:10.1016/j.crte.2012.10.008.
- Anthony, D. M., and D. E. Granger (2007), An empirical stream power formulation for knickpoint retreat in Appalachian Plateau fluviokarst, *Journal of Hydrology*, 343, 117–126, doi:10.1016/j.jhydrol.2007.06.013.
- Attal, M., P. A. Cowie, A. C. Whittaker, D. Hobley, G. E. Tucker, and G. P. Roberts (2011), Testing fluvial erosion models using the transient response of bedrock rivers to tectonic forcing in the Apennines, Italy, *Journal of Geophysical Research: Earth Surface*, 116(F2), F02,005, doi:10.1029/2010JF001875.
- Attal, M., S. M. Mudd, M. D. Hurst, B. Weinman, K. Yoo, and M. Naylor (2015), Impact of change in erosion rate and landscape steepness on hillslope and fluvial sediments grain size in the Feather River basin (Sierra Nevada, California), *Earth Surface Dynamics*, 3(1), 201–222, doi:10.5194/esurf-3-201-2015.

Braun, J., A. M. Heimsath, and J. Chappell (2001), Sediment transport mechanisms on soil-mantled hillslopes, *Geology*, *29*(8), 683–686, doi:10.1130/0091-7613(2001)029<0683:STMOSM>2.0.CO;2.

Carlston, C. W. (1963), *Drainage density and streamflow*, U.S. Govt. Print. Off.

Carson, M. A., and M. J. Kirkby (1972), *Hillslope Form and Process*, Cambridge University Press, Cambridge, UK.

Chorley, R. J., and M. A. Morgan (1962), Comparison of Morphometric Features, Unaka Mountains, Tennessee and North Carolina, and Dartmoor, England, *Geological Society of America Bulletin*, *73*(1), 17–34, doi:10.1130/0016-7606(1962)73[17:COMFUM]2.0.CO;2.

Church, M. (2006), Bed Material Transport and the Morphology of Alluvial River Channels, *Annual Review of Earth and Planetary Sciences*, *34*(1), 325–354, doi:10.1146/annurev.earth.33.092203.122721.

Clubb, F. J., S. M. Mudd, D. T. Milodowski, M. D. Hurst, and L. J. Slater (2014), Objective extraction of channel heads from high-resolution topographic data, *Water Resources Research*, *50*(5), 4283–4304, doi:10.1002/2013WR015167.

Dethier, D. P., W. Ouimet, P. R. Bierman, D. H. Rood, and G. Balco (2014), Basins and bedrock: Spatial variation in 10be erosion rates and increasing relief in the southern Rocky Mountains, USA, *Geology*, p. G34922.1, doi:10.1130/G34922.1.

DiBiase, R. A., K. X. Whipple, A. M. Heimsath, and W. B. Ouimet (2010), Landscape form and millennial erosion rates in the San Gabriel Mountains, CA, *Earth and Planetary Science Letters*, *289*(12), 134–144, doi:10.1016/j.epsl.2009.10.036.

DiBiase, R. A., A. M. Heimsath, and K. X. Whipple (2012), Hillslope response to tectonic forcing in threshold landscapes, *Earth Surface Processes and Landforms*, *37*(8), 855–865, doi:10.1002/esp.3205.

Finnegan, N. J., G. Roe, D. R. Montgomery, and B. Hallet (2005), Controls on the channel width of rivers: Implications for modeling fluvial incision of bedrock, *Geology*, *33*(3), 229–232, doi:10.1130/G21171.1.

Flint, J. J. (1974), Stream gradient as a function of order, magnitude, and discharge, *Water Resources Research*, *10*(5), 969–973, doi:10.1029/WR010i005p00969.

Furbish, D. J., P. K. Haff, W. E. Dietrich, and A. M. Heimsath (2009), Statistical description of slope-dependent soil transport and the diffusion-like coefficient, *Journal of Geophysical Research: Earth Surface*, *114*(F3), F00A05, doi:10.1029/2009JF001267.

Gabet, E. J., O. Reichman, and E. W. Seabloom (2003), The Effects of Bioturbation on Soil Processes and Sediment Transport, *Annual Review of Earth and Planetary Sciences*, *31*(1), 249–273, doi:10.1146/annurev.earth.31.100901.141314.

Gabet, E. J., S. M. Mudd, D. T. Milodowski, K. Yoo, M. D. Hurst, and A. Dosseto (2015), Local topography and erosion rate control regolith thickness along a ridge-line in the Sierra Nevada, California, *Earth Surface Processes and Landforms*, doi:10.1002/esp.3754.

Gasparini, N. M., and M. T. Brandon (2011), A generalized power law approximation for fluvial incision of bedrock channels, *Journal of Geophysical Research: Earth Surface*, *116*(F2), F02,020, doi:10.1029/2009JF001655.

Gregory, K. J., and D. E. Walling (1968), The Variation of Drainage Density Within a Catchment, *International Association of Scientific Hydrology. Bulletin*, *13*(2), 61–68,

doi:10.1080/02626666809493583.

Grieve, S. W., S. M. Mudd, and M. D. Hurst (2016a), How long is a hillslope?, *Earth Surface Processes and Landforms*, doi:10.1002/esp.3884.

Grieve, S. W. D., S. M. Mudd, M. D. Hurst, and D. T. Milodowski (2016b), A non-dimensional framework for exploring the relief structure of landscapes, *Earth Surface Dynamics*, 4(2), 309–325, doi:10.5194/esurf-4-309-2016.

Hack, J. (1973), Stream-profile analysis and stream-gradient index, *Journal of Research of the US Geological Survey*, 1(4), 421–429.

Harel, M. A., S. M. Mudd, and M. Attal (2016), Global analysis of the stream power law parameters based on worldwide 10be denudation rates, *Geomorphology*, 268, 184–196, doi:10.1016/j.geomorph.2016.05.035.

Heimsath, A. M., W. E. Dietrich, K. Nishiizumi, and R. C. Finkel (1997), The soil production function and landscape equilibrium, *Nature*, 388(6640), 358–361, doi:10.1038/41056.

Heimsath, A. M., D. J. Furbish, and W. E. Dietrich (2005), The illusion of diffusion: Field evidence for depth-dependent sediment transport, *Geology*, 33(12), 949–952, doi:10.1130/G21868.1.

Heimsath, A. M., R. A. DiBiase, and K. X. Whipple (2012), Soil production limits and the transition to bedrock-dominated landscapes, *Nature Geoscience*, 5(3), 210–214, doi:10.1038/ngeo1380.

Horton, R. E. (1945), Erosional Development of Streams and Their Drainage Basins; Hydrophysical Approach to Quantitative Morphology, *Geological Society of America Bulletin*, 56(3), 275–370, doi:10.1130/0016-7606(1945)56[275:EDOSAT]2.0.CO;2.

Howard, A. D. (1994), A detachment-limited model of drainage basin evolution, *Water Resources Research*, 30(7), 2261–2285, doi:10.1029/94WR00757.

Howard, A. D. (1997), Badland Morphology and Evolution: Interpretation Using a Simulation Model, *Earth Surface Processes and Landforms*, 22(3), 211–227, doi:10.1002/(SICI)1096-9837(199703)22:3<211::AID-ESP749>3.0.CO;2-E.

Howard, A. D., and G. Kerby (1983), Channel changes in badlands, *Geological Society of America Bulletin*, 94(6), 739–752, doi:10.1130/0016-7606(1983)94<739:CCIB>2.0.CO;2.

Hurst, M. D., S. M. Mudd, R. Walcott, M. Attal, and K. Yoo (2012), Using hilltop curvature to derive the spatial distribution of erosion rates, *Journal of Geophysical Research: Earth Surface*, 117(F2), doi:10.1029/2011JF002057.

Hurst, M. D., S. M. Mudd, M. Attal, and G. Hilley (2013a), Hillslopes Record the Growth and Decay of Landscapes, *Science*, 341(6148), 868–871, doi:10.1126/science.1241791.

Hurst, M. D., S. M. Mudd, K. Yoo, M. Attal, and R. Walcott (2013b), Influence of lithology on hillslope morphology and response to tectonic forcing in the northern Sierra Nevada of California, *Journal of Geophysical Research: Earth Surface*, 118(2), 832–851, doi:10.1002/jgrf.20049.

Istanbulluoglu, E., and R. L. Bras (2005), Vegetation-modulated landscape evolution: Effects of vegetation on landscape processes, drainage density, and topography, *Journal of Geophysical Research: Earth Surface*, 110(F2), doi:10.1029/2004JF000249.

Istanbulluoglu, E., D. G. Tarboton, R. T. Pack, and C. Luce (2003), A sediment transport model for incision of gullies on steep topography, *Water Resources Research*, 39(4), 1103, doi:10.1029/2002WR001467.

Kirkby, M. J. (1980), The stream head as a significant geomorphic threshold, in *Thresholds in Geomorphology*, edited by D. R. Coates and J. D. Vitek, pp. 53–73, Allen and Unwin, Winchester, Massachusetts.

Kirkby, M. J. (1993), Long term interactions between networks and hillslopes, in *Channel Network Hydrology*, edited by K. Beven and M. J. Kirkby, pp. 255–293, J. Wiley and Sons.

Lague, D. (2014), The stream power river incision model: evidence, theory and beyond, *Earth Surface Processes and Landforms*, 39(1), 38–61, doi:10.1002/esp.3462.

Lashermes, B., E. Foufoula-Georgiou, and W. E. Dietrich (2007), Channel network extraction from high resolution topography using wavelets, *Geophysical Research Letters*, 34(23), L23S04, doi:10.1029/2007GL031140.

Lavé, J., and J. P. Avouac (2001), Fluvial incision and tectonic uplift across the Himalayas of central Nepal, *Journal of Geophysical Research: Solid Earth*, 106(B11), 26,561–26,591, doi:10.1029/2001JB000359.

Leopold, L., and T. Maddock (1953), The hydraulic geometry of stream channels and some physiographic implications, *USGS Numbered Series 252*, United States Geological Survey.

Milodowski, D. T., S. M. Mudd, and E. T. A. Mitchard (2015a), Topographic roughness as a signature of the emergence of bedrock in eroding landscapes, *Earth Surface Dynamics*, 3(4), 483–499, doi:10.5194/esurf-3-483-2015.

Milodowski, D. T., S. M. Mudd, and E. T. A. Mitchard (2015b), Erosion rates as a potential bottom-up control of forest structural characteristics in the Sierra Nevada Mountains, *Ecology*, 96(1), 31–38, doi:10.1890/14-0649.1.

Montgomery, D. R., and W. E. Dietrich (1989), Source areas, drainage density, and channel initiation, *Water Resources Research*, 25(8), 1907–1918, doi:10.1029/WR025i008p01907.

Mudd, S. M., and D. J. Furbish (2007), Responses of soil-mantled hillslopes to transient channel incision rates, *Journal of Geophysical Research: Earth Surface*, 112(F3), F03S18, doi:10.1029/2006JF000516.

Mudd, S. M., M. Attal, D. T. Milodowski, S. W. Grieve, and D. A. Valters (2014), A statistical framework to quantify spatial variation in channel gradients using the integral method of channel profile analysis, *Journal of Geophysical Research: Earth Surface*, doi:10.1002/2013JF002981.

Oguchi, T. (1997), Drainage Density and Relative Relief in Humid Steep Mountains with Frequent Slope Failure, *Earth Surface Processes and Landforms*, 22(2), 107–120, doi:10.1002/(SICI)1096-9837(199702)22:2<107::AID-ESP680>3.0.CO;2-U.

Ouimet, W. B., K. X. Whipple, and D. E. Granger (2009), Beyond threshold hillslopes: Channel adjustment to base-level fall in tectonically active mountain ranges, *Geology*, 37(7), 579–582, doi:10.1130/G30013A.1.

Passalacqua, P., T. Do Trung, E. Foufoula-Georgiou, G. Sapiro, and W. E. Dietrich (2010a), A geometric framework for channel network extraction from lidar: Nonlinear diffusion and geodesic paths, *Journal of Geophysical Research: Earth Surface*, 115(F1), doi:10.1029/2009JF001254.

Passalacqua, P., P. Tarolli, and E. Foufoula-Georgiou (2010b), Testing space-scale methodologies for automatic geomorphic feature extraction from lidar in a complex mountainous landscape, *Water Resources Research*, 46(11), W11,535, doi:

10.1029/2009WR008812.

Passalacqua, P., P. Belmont, and E. Foufoula-Georgiou (2012), Automatic geomorphic feature extraction from lidar in flat and engineered landscapes, *Water Resources Research*, *48*(3), W03,528, doi:10.1029/2011WR010958.

Pelletier, J. D. (2010), Minimizing the grid-resolution dependence of flow-routing algorithms for geomorphic applications, *Geomorphology*, *122*(12), 91–98, doi:10.1016/j.geomorph.2010.06.001.

Pelletier, J. D. (2012), Fluvial and slope-wash erosion of soil-mantled landscapes: detachment- or transport-limited?, *Earth Surface Processes and Landforms*, *37*(1), 37–51, doi:10.1002/esp.2187.

Pelletier, J. D. (2013), A robust, two-parameter method for the extraction of drainage networks from high-resolution digital elevation models (DEMs): Evaluation using synthetic and real-world DEMs, *Water Resources Research*, *49*(1), 75–89, doi:10.1029/2012WR012452.

Pelletier, J. D., M. H. Nichols, and M. A. Nearing (2016), The influence of Holocene vegetation changes on topography and erosion rates: A case study at Walnut Gulch Experimental Watershed, Arizona, *Earth Surface Dynamics Discussions*, pp. 1–45, doi:10.5194/esurf-2016-3.

Perron, J. T., and L. Royden (2013), An integral approach to bedrock river profile analysis, *Earth Surface Processes and Landforms*, *38*(6), 570–576, doi:10.1002/esp.3302.

Perron, J. T., W. E. Dietrich, and J. W. Kirchner (2008), Controls on the spacing of first-order valleys, *Journal of Geophysical Research: Earth Surface*, *113*(F4), F04,016, doi:10.1029/2007JF000977.



Perron, J. T., J. W. Kirchner, and W. E. Dietrich (2009), Formation of evenly spaced ridges and valleys, *Nature*, *460*(7254), 502–505, doi:10.1038/nature08174.

Perron, J. T., P. W. Richardson, K. L. Ferrier, and M. Lapotre (2012), The root of branching river networks, *Nature*, *492*(7427), 100–103, doi:10.1038/nature11672.

Pritchard, D., G. G. Roberts, N. J. White, and C. N. Richardson (2009), Uplift histories from river profiles, *Geophysical Research Letters*, *36*(24), L24,301, doi:10.1029/2009GL040928.

Reinhardt, L. J., P. Bishop, T. B. Hoey, T. J. Dempster, and D. C. W. Sanderson (2007), Quantification of the transient response to base-level fall in a small mountain catchment: Sierra Nevada, southern Spain, *Journal of Geophysical Research: Earth Surface*, *112*(F3), F03S05, doi:10.1029/2006JF000524.

Riebe, C. S., J. W. Kirchner, D. E. Granger, and R. C. Finkel (2000), Erosional equilibrium and disequilibrium in the Sierra Nevada, inferred from cosmogenic <sup>26</sup>Al and <sup>10</sup>Be in alluvial sediment, *Geology*, *28*(9), 803–806, doi:10.1130/0091-7613(2000)28<803:EEADIT>2.0.CO;2.

Riebe, C. S., L. S. Sklar, C. E. Lukens, and D. L. Shuster (2015), Climate and topography control the size and flux of sediment produced on steep mountain slopes, *Proceedings of the National Academy of Sciences*, *112*(51), 15,574–15,579, doi:10.1073/pnas.1503567112.

Roberts, G. G., and N. White (2010), Estimating uplift rate histories from river profiles using African examples, *Journal of Geophysical Research: Solid Earth*, *115*(B2), B02,406, doi:10.1029/2009JB006692.

Roering, J. J. (2008), How well can hillslope evolution models explain topography? Simulating soil transport and production with high-resolution topographic data, *Geological Society of America Bulletin*, 120(9-10), 1248–1262, doi:10.1130/B26283.1.

Roering, J. J., J. W. Kirchner, and W. E. Dietrich (1999), Evidence for nonlinear, diffusive sediment transport on hillslopes and implications for landscape morphology, *Water Resources Research*, 35(3), 853–870, doi:10.1029/1998WR900090.

Roering, J. J., J. W. Kirchner, L. S. Sklar, and W. E. Dietrich (2001), Hillslope evolution by nonlinear creep and landsliding: An experimental study, *Geology*, 29(2), 143–146, doi:10.1130/0091-7613(2001)029;0143:HEBNCA;2.0.CO;2.

Roering, J. J., J. T. Perron, and J. W. Kirchner (2007), Functional relationships between denudation and hillslope form and relief, *Earth and Planetary Science Letters*, 264(12), 245–258, doi:10.1016/j.epsl.2007.09.035.

Roering, J. J., J. Marshall, A. M. Booth, M. Mort, and Q. Jin (2010), Evidence for biotic controls on topography and soil production, *Earth and Planetary Science Letters*, 298(12), 183–190, doi:10.1016/j.epsl.2010.07.040.

Royden, L., and J. T. Perron (2013), Solutions of the stream power equation and application to the evolution of river longitudinal profiles, *Journal of Geophysical Research: Earth Surface*, 118(2), 497–518, doi:10.1002/jgrf.20031.

Sangireddy, H., R. A. Carothers, C. P. Stark, and P. Passalacqua (2016), Controls of climate, topography, vegetation, and lithology on drainage density extracted from high resolution topography data, *Journal of Hydrology*, 537, 271–282, doi:10.1016/j.jhydrol.2016.02.051.

Simpson, G., and F. Schlunegger (2003), Topographic evolution and morphology of surfaces evolving in response to coupled fluvial and hillslope sediment transport, *Journal of Geophysical Research: Solid Earth*, 108(B6), 2300, doi:10.1029/2002JB002162.

Sklar, L., and W. E. Dietrich (1998), River Longitudinal Profiles and Bedrock Incision Models: Stream Power and the Influence of Sediment Supply, in *Rivers Over Rock: Fluvial Processes in Bedrock Channels*, edited by K. J. Tinkler and E. E. Wohl, pp. 237–260, American Geophysical Union.

Snyder, N. P., K. X. Whipple, G. E. Tucker, and D. J. Merritts (2000), Landscape response to tectonic forcing: Digital elevation model analysis of stream profiles in the Mendocino triple junction region, northern California, *Geological Society of America Bulletin*, 112(8), 1250–1263, doi:10.1130/0016-7606(2000)112<1250:LRTTFD>2.0.CO;2.

Stock, J., and W. E. Dietrich (2003), Valley incision by debris flows: Evidence of a topographic signature, *Water Resources Research*, 39(4), doi:10.1029/2001WR001057.

Stock, J. D., and D. R. Montgomery (1999), Geologic constraints on bedrock river incision using the stream power law, *Journal of Geophysical Research: Solid Earth*, 104(B3), 4983–4993, doi:10.1029/98JB02139.

Sweeney, K. E., J. J. Roering, and C. Ellis (2015), Experimental evidence for hillslope control of landscape scale, *Science*, 349(6243), 51–53, doi:10.1126/science.aab0017.

Talling, P. J., and M. J. Sowter (1999), Drainage density on progressively tilted surfaces with different gradients, Wheeler Ridge, California, *Earth Surface Processes and Landforms*, 24(9), 809–824, doi:10.1002/(SICI)1096-9837(199908)24:9<809::AID-ESP13>3.0.CO;2-R.

Tarboton, D. G., R. L. Bras, and I. Rodriguez-Iturbe (1992), A physical basis for drainage density, *Geomorphology*, *5*(12), 59–76, doi:10.1016/0169-555X(92)90058-V.

Tucker, G., S. Lancaster, N. Gasparini, and R. Bras (2001), The Channel-Hillslope Integrated Landscape Development Model (CHILD), in *Landscape Erosion and Evolution Modeling*, edited by R. S. Harmon and W. W. D. III, pp. 349–388, Springer US, doi:10.1007/978-1-4615-0575-4\_12.

Tucker, G. E., and R. L. Bras (1998), Hillslope processes, drainage density, and landscape morphology, *Water Resources Research*, *34*(10), 2751–2764, doi:10.1029/98WR01474.

Whipple, K. X., and G. E. Tucker (1999), Dynamics of the stream-power river incision model: Implications for height limits of mountain ranges, landscape response timescales, and research needs, *Journal of Geophysical Research: Solid Earth*, *104*(B8), 17,661–17,674, doi:10.1029/1999JB900120.

Whipple, K. X., G. S. Hancock, and R. S. Anderson (2000), River incision into bedrock: Mechanics and relative efficacy of plucking, abrasion, and cavitation, *Geological Society of America Bulletin*, *112*(3), 490–503, doi:10.1130/0016-7606(2000)112<490:RIIBMA>2.0.CO;2.

Whittaker, A. C., and S. J. Boulton (2012), Tectonic and climatic controls on knickpoint retreat rates and landscape response times, *Journal of Geophysical Research: Earth Surface*, *117*(F2), F02,024, doi:10.1029/2011JF002157.

Whittaker, A. C., M. Attal, P. A. Cowie, G. E. Tucker, and G. Roberts (2008), Decoding temporal and spatial patterns of fault uplift using transient river long profiles, *Geomorphology*, *100*(34), 506–526, doi:10.1016/j.geomorph.2008.01.018.

Willgoose, G., R. L. Bras, and I. Rodriguez-Iturbe (1991), A coupled channel network growth and hillslope evolution model: 1. Theory, *Water Resources Research*, *27*(7), 1671–1684, doi:10.1029/91WR00935.

Wobus, C., K. X. Whipple, E. Kirby, N. Snyder, J. Johnson, K. Spyropolou, B. Crosby, and D. Sheehan (2006), Tectonics from topography: Procedures, promise, and pitfalls, *Geological Society of America Special Papers*, *398*, 55–74, doi:10.1130/2006.2398(04).

Yoo, K., R. Amundson, A. M. Heimsath, and W. E. Dietrich (2005), Process-based model linking pocket gopher (*Thomomys bottae*) activity to sediment transport and soil thickness, *Geology*, *33*(11), 917–920, doi:10.1130/G21831.1.

**Table 1.** Parameter values chosen for CHILD model runs

Parameter	Value	Justification
Mean precipitation rate	0.75 mm hr <sup>-1</sup>	Preserved from <i>Mudd et al.</i> [2014]
Mean storm duration	22 h	Preserved from <i>Mudd et al.</i> [2014]
Mean interstorm duration	260 h	Preserved from <i>Mudd et al.</i> [2014]
Specific weight of water, $k_t$	9810 kg m <sup>-2</sup> s <sup>-2</sup>	Preserved from <i>Mudd et al.</i> [2014]
Channel width coefficient, $k_w$	4.6 m <sup>-1/2</sup> s <sup>1/2</sup>	Preserved from <i>Mudd et al.</i> [2014]
Erodibility coefficient, $k_b$	$1 \times 10^{-4}$ m yr <sup>-1</sup> (W m <sup>-2</sup> ) <sup>-1</sup>	Adjusted from <i>Mudd et al.</i> [2014] to account for varying $n$ values
Hillslope transport coefficient, $D$	0.0088 m <sup>2</sup> yr <sup>-1</sup>	Calculated by <i>Hurst et al.</i> [2013b] for Feather River CA
Critical slope $S_c$ (nonlinear runs)	1.25	Calculated by <i>Roering et al.</i> [1999] for Oregon Coast Range

**Table 2.** Details of climate and lithology for each field site<sup>1</sup>

Field site	UTM Zone	MAP (mm)	MAT (°C)	Lithology	Elevations (m AMSL)	Soil ridgetops (%) <sup>2</sup>	Difference in gradient (%) <sup>3</sup>
Feather River, CA	10N	1796	13.8	Granite, granodiorites, tonalite	225-1549	94	24.3
San Gabriel Mts, CA	11N	685	13.7	Granite	1076-2010	87	19.5
Boulder Creek, CO	13N	566	5.9	Gneiss and granite	1652-3519	85	13.8
Guadalupe Mts, NM	13N	454	13.5	Limestone, dolomite	1536-1980	98	9.9
Bitterroot National Forest, ID	11N	830	3.9	Mica schist and gneiss	816-2497	70	11.3

<sup>1</sup> MAP = mean annual precipitation; MAT = mean annual temperature [PRISM Climate Group]

<sup>2</sup> Calculated following *Milodowski et al.* [2015a]

<sup>3</sup> Mean percentage difference between gradients 2 m above and below channel heads

**Table 3.** Compiled CRN samples from Feather River, CA, and Boulder Creek, CO<sup>1</sup>

Field site	Basin ID	Easting	Northing	Erosion rate (mm/kyr)	Standard deviation (mm/kyr)	Author
FR	FR-2	640504.27	4391321.67	125.9	23.2	Hurst et al. 2012
FR	FR-4	647490.78	4388656.03	253.8	66.6	Hurst et al. 2012
FR	FR-5	648350.75	4388752.06	133.3	31.9	Hurst et al. 2012
FR	FR-6	643053.99	4388961.32	25.2	2.7	Hurst et al. 2012
FR	FR-7	643117.49	4389018.47	18.5	2.0	Hurst et al. 2012
FR	FR-8	643790.59	4391155.89	12.5	1.4	Hurst et al. 2012
FR	FR-9	643346.09	4390768.54	14.4	1.6	Hurst et al. 2012
FR	FR-10	642298.33	4389824.92	24.3	2.7	Hurst et al. 2012
FR	BRB-2	645334.53	4389864.62	38.6	3.4	Hurst et al. 2012
FR	BRB-6	645336.52	4389843.51	35.7	4.7	Hurst et al. 2012
FR	BRB-8	645547.44	4390101.49	90.3	8.5	Hurst et al. 2012
FR	BEAN-1	643390.54	4386092.39	43.8	3.7	Hurst et al. 2012
FR	BEAN-2	643479.44	4387197.29	44.8	3.7	Hurst et al. 2012
FR	BEAN-4	643536.59	4387349.69	65	5.3	Hurst et al. 2012
FR	BEAN-5	643333.39	4388156.14	45.1	3.8	Hurst et al. 2012
FR	BEAN-7	643511.19	4387851.34	90.7	7.2	Hurst et al. 2012
FR	FT-3	644875.52	4392651.31	26.2	2.3	Hurst et al. 2012
FR	FT-4	644872.88	4392628.56	24.9	2.2	Hurst et al. 2012
FR	FT-6	644462.24	4393416.23	23.6	2.1	Hurst et al. 2012
FR	BS-1	650229.72	4397969.15	99.9	9.7	Riebe et al. 2000
FR	SB-1	650758.89	4398041.91	75.4	6.6	Riebe et al. 2000
BC	DC-01-01	459127.15	4424213.09	31.4	2.56	Dethier et al. 2014
BC	DC-01-03	470265.96	4411862.60	18.48	1.55	Dethier et al. 2014
BC	DC-01-04	463608.27	4401576.01	23.3	1.96	Dethier et al. 2014
BC	DC-01-05	471610.16	4399252.56	20.72	1.78	Dethier et al. 2014
BC	DC-01-06	465526.88	4423375.63	32.77	2.7	Dethier et al. 2014
BC	DC-01-09	459882.61	4445285.94	18.98	1.6	Dethier et al. 2014
BC	DC-01-11	472690.03	4450295.82	22.39	1.88	Dethier et al. 2014
BC	DC-01-12	467600.04	4459486.53	14.86	1.26	Dethier et al. 2014
BC	DC-01-14	466043.22	4473501.55	17.14	1.45	Dethier et al. 2014
BC	DC-01-16	470649.89	4503943.49	21.62	1.78	Dethier et al. 2014
BC	DC-01-19	347619.84	4466934.06	29.51	2.43	Dethier et al. 2014
BC	OW-01-07	337088.69	4568762.91	30.75	2.57	Dethier et al. 2014
BC	JFC-02-03	429688.04	4450427.15	37.67	3.35	Dethier et al. 2014
BC	MJ-BC-01	445725.68	4421257.71	19.48	1.68	Dethier et al. 2014
BC	MJ-BC-17	449479.18	4433367.11	28.94	2.41	Dethier et al. 2014
BC	JFW-02-13	471124.81	4562497.45	22.81	1.92	Dethier et al. 2014
BC	DC-09-18	460869.07	4429299.65	19.41	1.58	Dethier et al. 2014
BC	DC-09-20	459448.16	4429799.91	14.97	1.25	Dethier et al. 2014
BC	DC-01-17	427084.65	4525460.09	37.11	3.02	Dethier et al. 2014
BC	DC-01-18	343228.15	4477463.60	47.58	3.85	Dethier et al. 2014
BC	OW-01-08	384303.27	4695037.67	286.62	31.09	Dethier et al. 2014

<sup>1</sup> FR = Feather River, UTM Zone 10N; BC = Boulder Creek, UTM Zone 13N.



**Table 4.** Calculated best-fit  $m/n$  ratios for each field site

Field site	Mean $m/n$	Median $m/n$	Standard deviation
Feather River, CA	0.30	0.25	0.141
San Gabriel Mountains, CA	0.42	0.438	0.146
Boulder Creek, CO	0.42	0.425	0.037
Guadalupe Mountains, NM	0.39	0.275	0.129
Bitterroot National Forest, ID	0.31	0.325	0.02

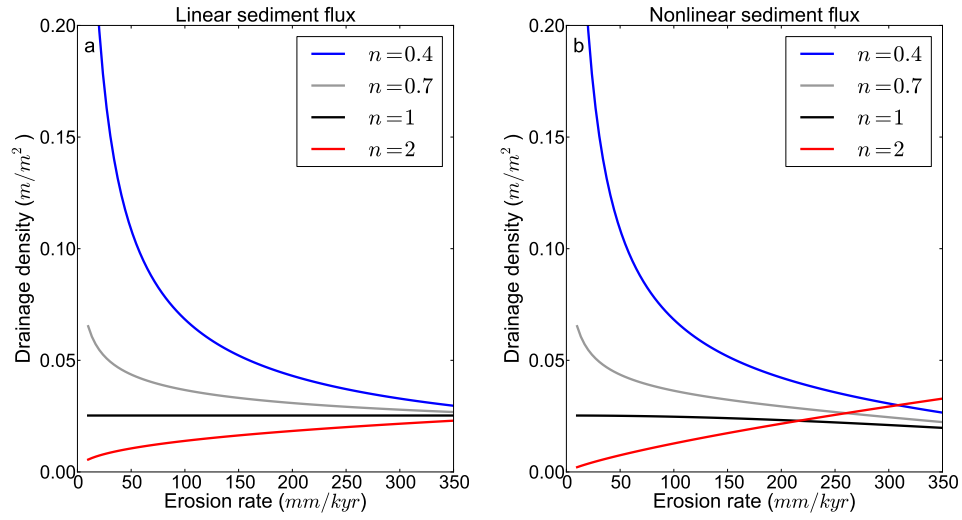


**Figure 1.** Analytical predictions of the relationship between drainage density and erosion rate for a) linear hillslope sediment flux, b) nonlinear hillslope sediment flux. We set parameters in equations (6) and (8) to the following:  $D = 0.0088 \text{ m}^2 \text{ yr}^{-1}$ ,  $K = 1 \times 10^{-4} \text{ m yr}^{-1}$ ,  $m = 0.5$ , and  $S_c = 1.25$ . The values of these parameters are the same as for the numerical modeling runs (Table 1). The relationship depends on the value of  $n$  in the stream power law: we predict a positive relationship for  $n > 1$ , a negative relationship for  $n < 1$ , and no relationship between  $D_d$  and  $E$  for  $n = 1$ .

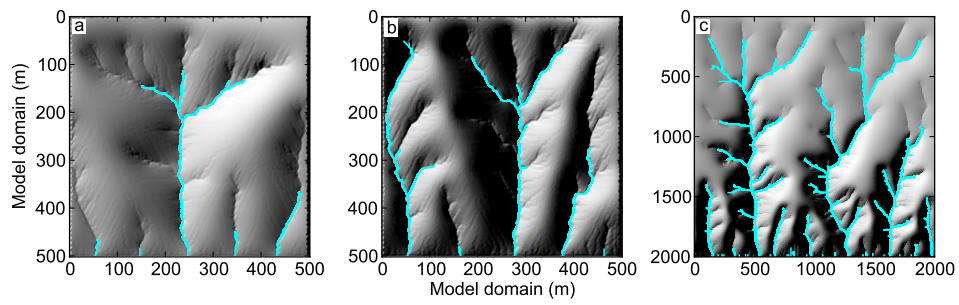


**Figure 2.** Example of topography and channel networks extracted from CHILD runs for  $n = 2$ . The lower boundary of the model is fixed, with the other boundaries set to no flux. a) Steady state run with  $U = 110$  mm/kyr, maximum elevation of 163 m. b) Steady state run with  $U = 320$  mm/kyr, maximum elevation of 351 m. c) Transient run with  $U = 40$  mm/kyr for 60 Ma then increased to 320 mm/kyr for 1 Ma, maximum elevation of 595 m.

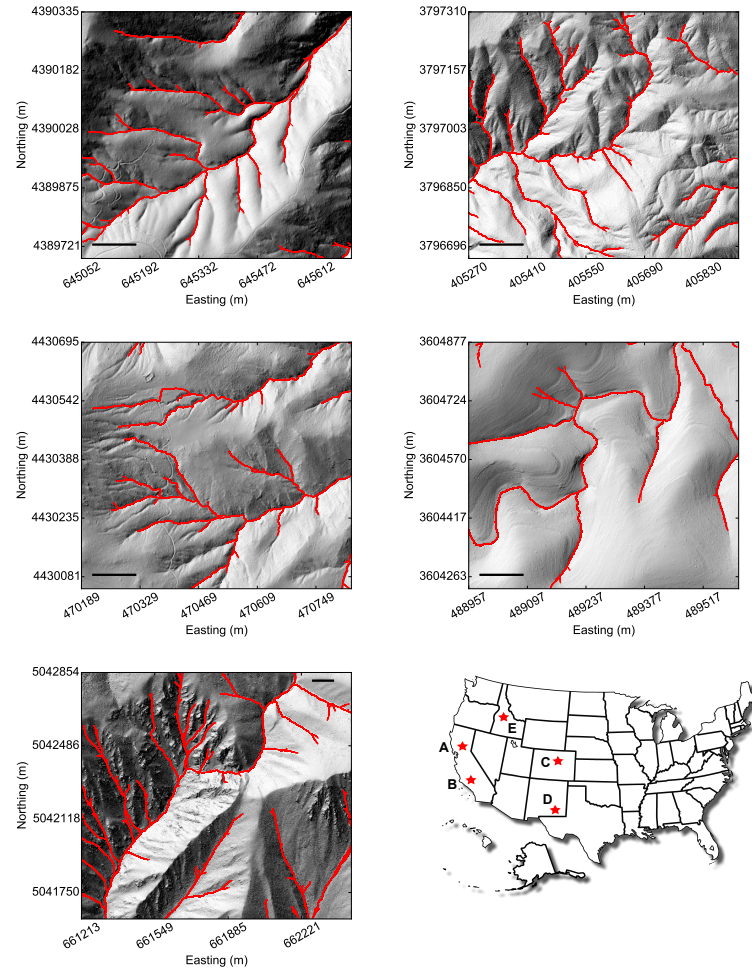


**Figure 3.** Shaded relief maps of part of each field site with drainage network extracted using the DrEICH algorithm. The scale bar on each map is 100 m. a) Feather River, CA. UTM Zone 10N. b) San Gabriel Mountains, CA. UTM Zone 11N. c) Boulder Creek, CO. UTM Zone 13N. d) Guadalupe Mountains, NM. UTM Zone 13N. e) Bitterroot National Forest, ID, UTM Zone 11N. f) USA state map showing location of field sites a-e.

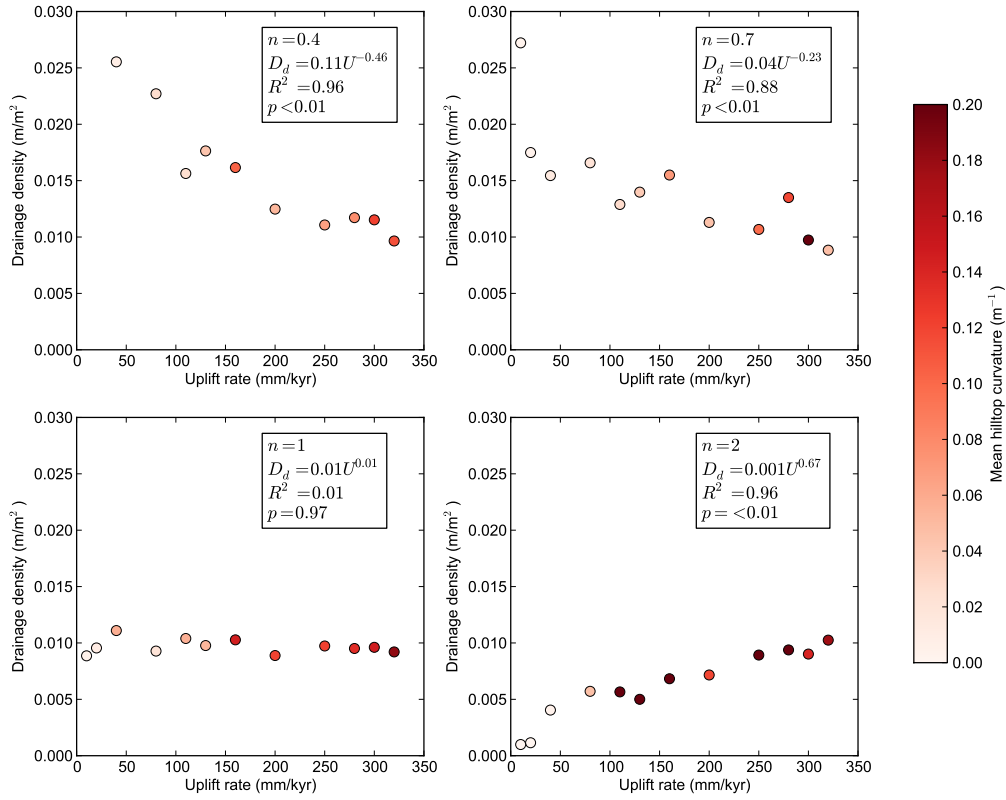


**Figure 4.** Results of CHILD modeling for steady state scenarios with linear hillslope sediment transport. Plots indicate measured relationship between drainage density and uplift rate where  $n = 0.4$ ,  $n = 0.7$ ,  $n = 1$ , and  $n = 2$ . The points are colored by mean hilltop curvature: lighter colors indicate low curvature values and darker colors indicate high values.

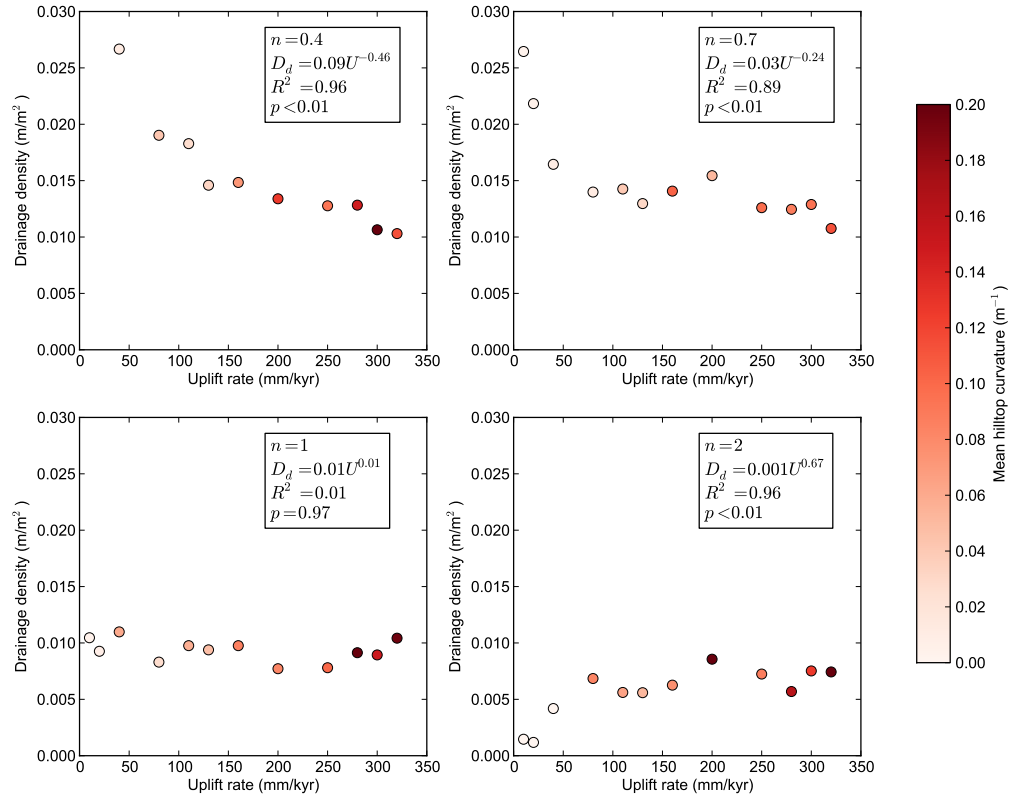


**Figure 5.** Results of CHILD modeling for steady state scenarios with non-linear hillslope sediment transport. Plots indicate measured relationship between drainage density and uplift rate where  $n = 0.4$ ,  $n = 0.7$ ,  $n = 1$ , and  $n = 2$ . The points are colored by mean hilltop curvature: lighter colors indicate low curvature values and darker colors indicate high values.

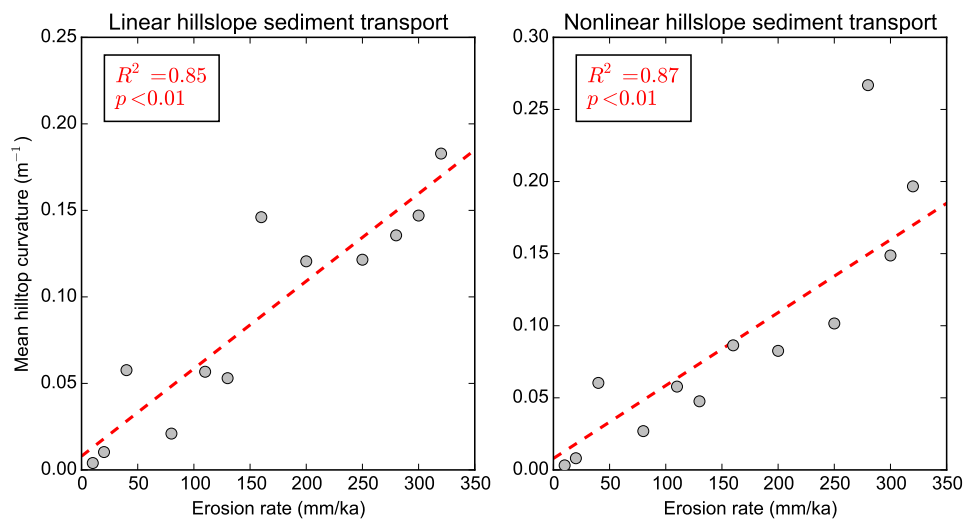


**Figure 6.** Scatter plots of mean hilltop curvature against uplift rate for steady-state CHILD modeling scenarios where  $n = 1$ , showing both linear and non-linear hillslope sediment flux. A significant positive linear relationship is found for both sediment transport scenarios, with  $R^2$  values of 0.85 and 0.87 respectively.

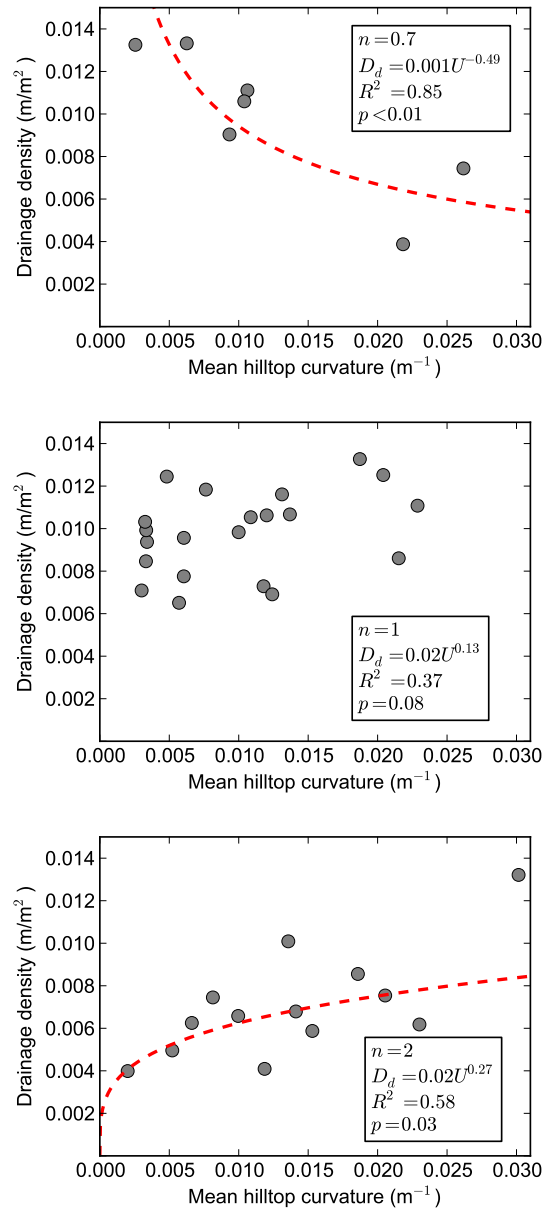


**Figure 7.** Results of CHILD modeling for transient scenarios with linear hillslope sediment flux. Plots indicate measured relationship between drainage density and mean hilltop curvature where  $n = 0.7$ ,  $n = 1$ , and  $n = 2$ .



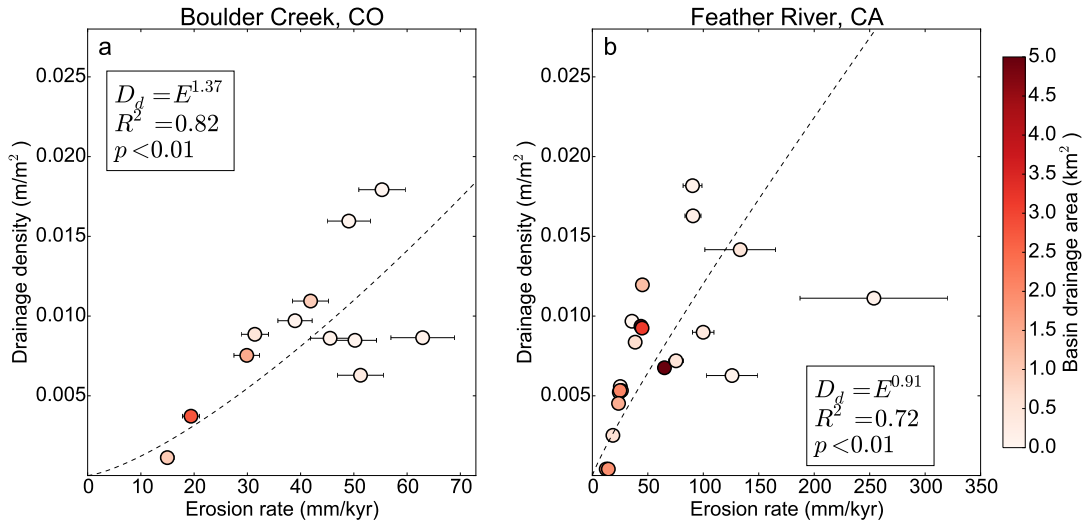


**Figure 8.** Scatterplots showing relationship between CRN-derived erosion rate and drainage density ( $D_d$ ) with a fitted power-law relationship. The  $R^2$  and  $p$  value of the regressions are also shown. The points are coloured based on the contributing area of the basin, with white representing low contributing areas and dark red representing high contributing areas. a) Scatterplot for the Boulder Creek field site, Colorado. b) Scatterplot for the Feather River field site, California.

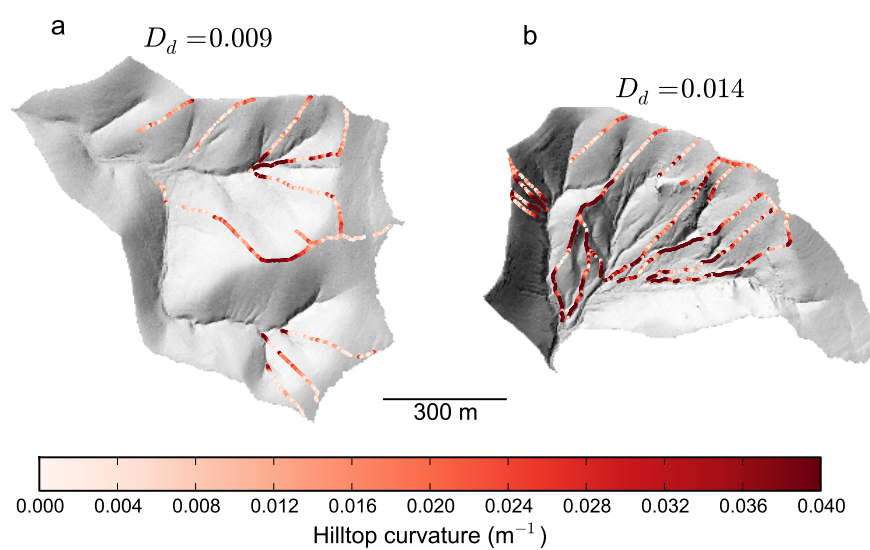


**Figure 9.** Shaded relief map showing spatial distribution of mean hilltop curvature across Guadalupe Mountains, NM for a) a low drainage density basin, and b) a high drainage density basin. The hilltop curvature is shown in red.

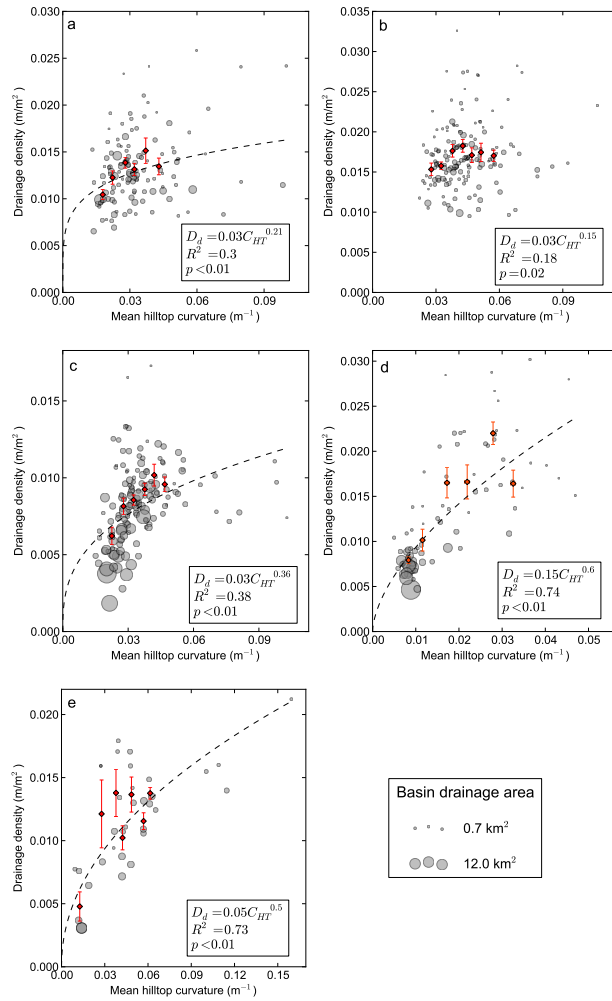


**Figure 10.** Scatterplots of the relationship between mean  $C_{HT}$  and  $D_d$  for each field site. The full dataset is shown in grey, with the size of the points representing the contributing area. The binned data are shown in red, with a bin width of  $0.005 \text{ m}^{-1}$ . A polynomial fit of the full dataset is represented by the dashed line. a) Feather River, CA. b) San Gabriel Mountains, CA. c) Boulder Creek, CO. d) Guadalupe Mountains, NM. e) Bitterroot National Forest, ID.

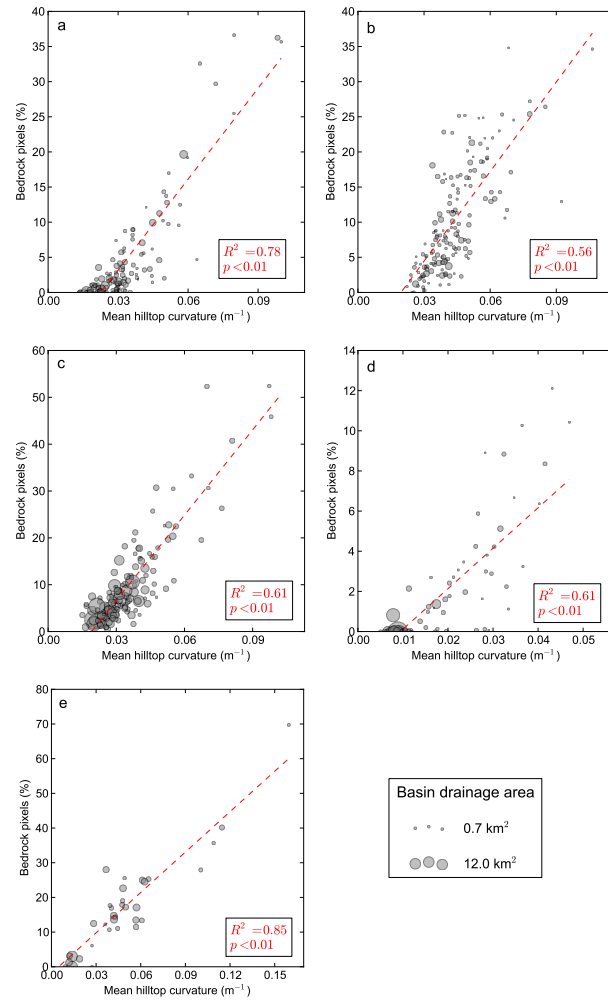


**Figure 11.** Scatterplots of the relationship between mean  $C_{HT}$  and the percentage of ridgetops identified as bedrock for third order basins in each field site. The size of the points represents the contributing area of the basin, and the dashed line shows a linear regression through the dataset. a) Feather River, CA. b) San Gabriel Mountains, CA. c) Boulder Creek, CO. d) Guadalupe Mountains, NM. e) Bitterroot National Forest, ID.